

**Evaluation of NU-WRF Performance on Air Quality Simulation under Various Model Resolutions –
An Investigation within Framework of MICS-Asia Phase III
By Z. Tao et al.**

The authors greatly appreciate the reviewers' insightful and constructive comments. We have made substantial revisions in an effort to address the key comments. The following lists our responses (plain text) to the reviewer's comments (bold).

Response to Reviewer #1

1. The simulations conducted over the three nested domains are used in this study for comparisons and evaluations of meteorological and air quality simulations among three different grid-spacings. The way of nesting used in the simulations may have a large impact on the sensitivity of simulation results to grid spacing. Which nesting way is used in the simulations? One-way nesting or two-way nesting? If two-way nesting is selected in the simulations which I doubt according to results presented in the manuscript (e.g., L175-176), how your conclusion or findings can be affected by this selection?

In this study, we chose the one-way nesting approach. If a two-way nesting approach is used, the meteorological fields for the study domain (innermost domain) from 3 horizontal resolutions would be very similar to each other, which would obscure the conclusion of the effect of model resolution on air quality. In the one-way nesting approach, the meteorological fields of the mother domains are independent on those of the respective nested domains, thus representing a cleaner signal of the grid resolution effect on air quality than that of the two-way nesting approach. As illustrated in Figure 6 of the manuscript, surface wind, temperature, PBLH, ground-level short wave radiation, and cloud water path out of each grid display noticeable differences. Due to the resource constrain, this investigation chose the one-way nesting approach, in which the lateral boundary conditions (LBCs) for each grid modeling were not identical. A “cleaner” approach would be to apply the identical LBCs out of the global model to drive NU-WRF under various grid resolutions to evaluate their impacts on air quality. However, we do not anticipate that such “cleaner” approach would remarkably alter the results based on the one-way nesting approach. In the manuscript, we added a statement in section 2 that the one-way nesting was utilized.

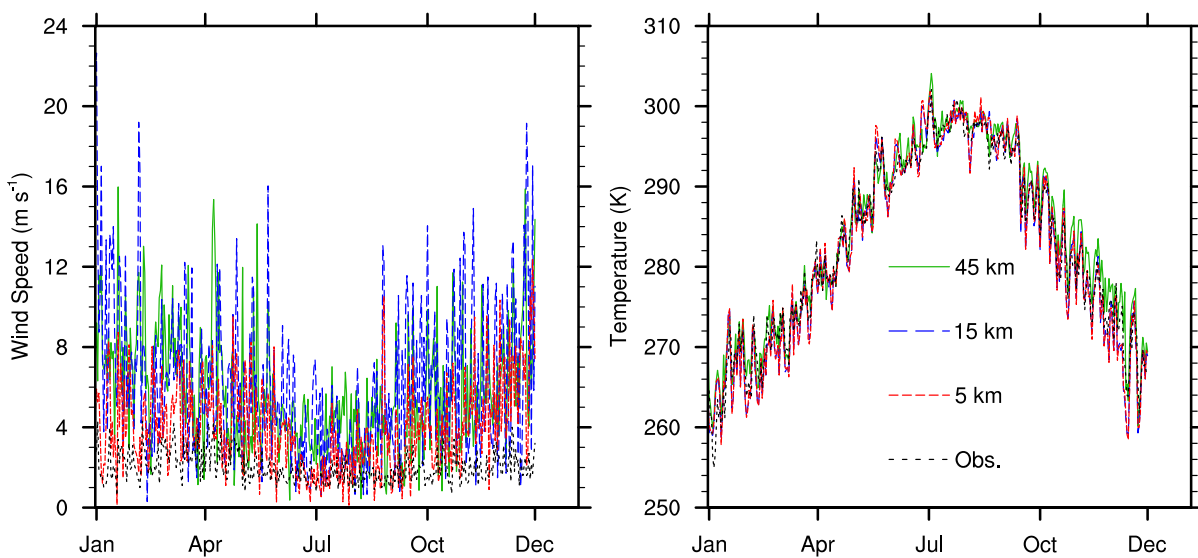
“...A one-way nesting approach was applied so that the values of the mother domains were independent on those of the respective nested domains...”

2. The impact of grid-spacing on met or air quality simulations is highly dependent on terrain complexity of the study region. Given the relatively flat terrain of North China Plain (NCP), the impact of the grid-spacing on the simulations over land cannot be as large as expected. We believe that complex terrain and the situations with a large surface-cover contrast such as coastal regions do require high-resolution simulations. 15-km horizontal resolution that the authors suggest for the MICS-Asia study is definitely not enough to resolve the detailed local wind structures such as land-sea breeze or lake-breeze over the coastal regions which many large cities (e.g., Shanghai and Hong Kong) are located and air pollution is a big concern. It would be very helpful if the authors can shed little bit

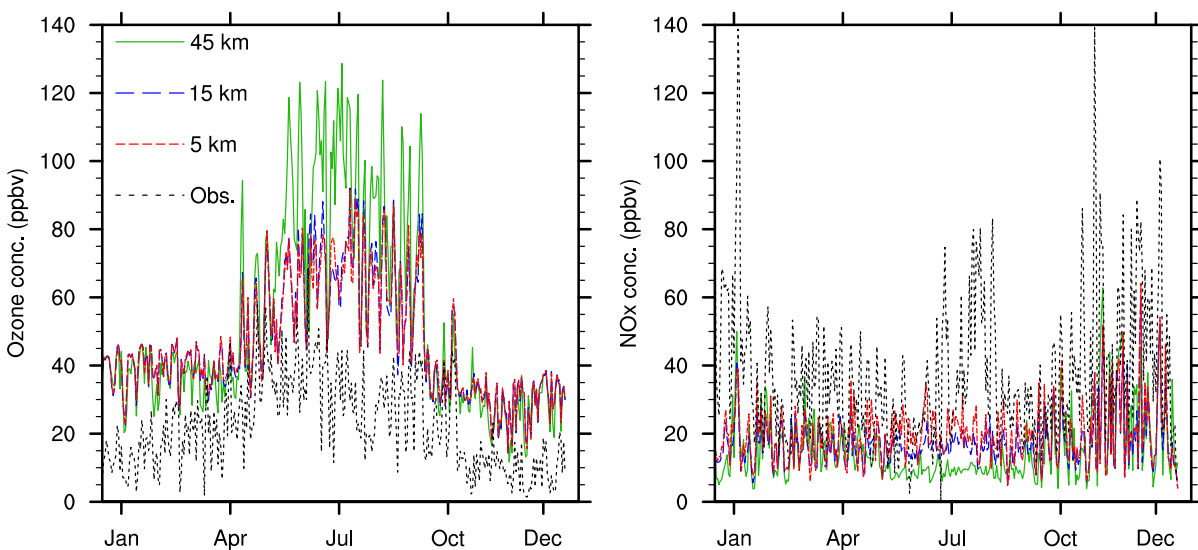
light on discussion of model performance with three grid-spacings at those sites along or near coastal regions.

In this investigation, we have found that the 5-km resolution modeling provided the best results of wind and surface pollutant levels, especially in polluted conditions that were the most relevant to air quality regulation (e.g., compliance of national air quality standards), measured by bias and RMSE. However, the improvement of model performance on air quality was not linear with the resolution increase. For example, the accuracy of modeled surface O₃ out of the 15-km grid was greatly improved over the one from the 45-km grid. Further increase of grid resolution to 5-km, however, showed diminished impact on model performance improvement on O₃ prediction for the study region. In addition, the cost in terms of cpu hours and disk space usage increased dramatically when adopting the 5-km grid, which would be a big hurdle for the inter-model comparison studies such as MICS-Asia that relied on community contributions to model Asia air quality over a relatively long time period. Considering all these factors, we suggest a 15-km resolution grid for future MICS-Asia modeling activity to achieve both accuracy and efficiency.

Of course, the choice of grid resolution also depends on the problems to be solved, such as air quality over coastal areas which show sharp contrasts of surface roughness, albedo, and thermal characteristics. In this investigation, QHD site locates approximately 5 km from the ocean and is subject to sea breeze effects. The temporal profiles of surface wind speed and temperature from the observation and model results out of 3 grids for QHD are shown in the following figure. The results indicated that the choice of grid resolution had large impacts on model simulations at this coastal site. The selection of the 5-km grid reduced biases of both surface temperature and wind speed. The biases of temperature reduced from 1.22 K (45-km) to -0.42 K (15-km), and further down to -0.31 K when the 5-km grid was applied. The biases of surface wind speed for the 45-km, 15-km, and 5-km grids were 3.72, 4.19, and 1.95 m s⁻¹, respectively. Since there were no hourly wind data available to this study, the diurnal changes of sea breeze cannot be evaluated. However, the benefit of finer resolution grid to improving wind simulation was obvious.



The following figure displays the time evolution of surface ozone and NO_x concentrations from the observation and model results out of 3 grids for QHD. It can be seen that overall the model, regardless which grid resolution was applied, underestimated ground-level NO_x concentrations but overestimated surface ozone levels. The ozone overestimate was especially large during summer months when its photochemical formation was the most efficient. We believe that the inaccurate NO_x emissions representations were largely responsible for the model-observation mismatch. On the other hand, the benefit of increasing grid resolution to improving ozone and NO_x forecast skills was obvious. The biases of ozone/NO_x for the 45-km, 15-km, and 5-km resolution grids were 29.94/-22.46 ppbv, 24.09/-20.29 ppbv, 23.97/-17.95 ppbv, respectively. The respective RMSE were 37.24/28.87 ppbv, 27.28/27.57 ppbv, 27.01/26.38 ppbv. The improvement using the 15-km grid over the 45-km grid was remarkable but that using the 5-km grid over the 15-km grid was marginal.



In summary, the authors agree that, in general, the higher the grid resolution is, the better the simulation results will be. High resolution modeling is especially important to coastal areas and complex terrains where land-surface driving forces are in sharp contrast, such as QHD site. On the other hand, this research also agrees with the findings reported in many other papers that the benefit of higher resolution modeling of air quality starts to diminish at certain point due to the nonlinear nature of the atmospheric system. Balancing the modeling accuracy and computing resource constrain, a 15-km resolution grid has been recommended for future MICS-Asia activities if the investigate domain remains unchanged. We modified the manuscript to make this point explicitly stated in the section 3.1.2.b (Individual site) section 4 (Summary).

In section 3.1.2.b:

“An effort has been put to identify the potential reasons that caused the model-observation discrepancy. First and as discussed previously, the spatial distribution of emissions was one key to determining air quality forecast accuracy. Figure 3s shows the typical time evolutions of surface O₃ and NO_x over the rural (XL) and

urban (QHD) sites. It can readily be seen that NO_x was underestimated at the urban site but overestimated at the rural site. The coarser the grid resolution, the severer the underestimates/overestimates were. This indicated that the 45-km resolution tended to smooth out emissions to make urban (or emissions centers) less polluted but rural more polluted. It in turn led to an overestimate of surface O₃ over the urban sites mainly due to the reduced NO_x titration effect, especially at night when there was no photochemical O₃ formation. The statistics showed that the bias of the modeled daytime (7 am ~ 7 pm local time) average surface O₃ was 30% ~ 90% smaller than that of the daily average in the urban sites, no matter which grid resolution was applied. This suggested that in the future the high-resolution emissions, especially proper representation of emission gradients, would be helpful in improving air quality prediction. The effect of emissions gradients associated with the grid resolution would be further discussed in the inter-model comparison section.

Next, the driving meteorology, especially wind, was important to accurately forecast air quality over coastal areas that bore sharp thermal contrasts. QHD site locates approximately 5 km from the ocean and is subject to sea breeze effects. The detailed analysis of meteorology and air quality over QHD was conducted. The results indicated that the choice of grid resolution had large impacts on model simulations at this coastal site. The selection of the 5-km grid reduced biases of both surface temperature and wind speed. The biases of temperature reduced from 1.22 K (45-km) to -0.42 K (15-km), and further down to -0.31 K when the 5-km grid was applied. The biases of surface wind speed for the 45-km, 15-km, and 5-km grids were 3.72, 4.19, and 1.95 m s⁻¹, respectively. The improvement of meteorology forecast helped reducing the biases of air quality modeling. The biases of O₃/NO_x for the 45-km, 15-km, and 5-km resolution grids were 29.94/-22.46 ppbv, 24.09/-20.29 ppbv, 23.97/-17.95 ppbv, respectively. The improvement using the 15-km grid over the 45-km grid was remarkable but that using the 5-km grid over the 15-km grid was marginal. The result emphasized the importance of high-resolution modeling to improvements of air quality forecast skills, especially at coastal and complex terrain areas (e.g., QHD and XL).”

In section 4:

“...With regard to MICS-Asia Phase III whose major goal was to examine regional air quality, in general, the finer the grid resolution was, the better the simulation results would be. This was especially true over the coastal areas and complex terrains where a sharp local energy gradient existed. Fine resolution grid was also extremely helpful to reproducing pollutants at higher concentrations that were most relevant to air quality planning and management. However, the benefit of high resolution was not linear with the decrease of grid size. At certain point, the improved modeling accuracy due to an increase in grid resolution was so marginal that it cannot justify the computational cost associated with the fine grid simulation. Based on the balance of modeling accuracy and efficiency, a 15-km horizontal grid appeared to be an appropriate choice to optimize model performance and resource usage if the study domain remained unchanged for future MICS-Asia activities. The study suggested that the high-resolution emissions, especially the proper representation of emission gradients, would be helpful in improving air quality prediction. Moreover, the profile measurements of both meteorology and air quality, in supplement with the ground monitoring networks, would be greatly helpful to identifying model deficiencies and thus improving model forecast skills”

3. Taylor diagram (Figure 2) is a useful way to present model performance, but it is not enough to represent model performance over a large region such as NCP and long- time simulation period such as one year since model performs differently in different sub-regions like urban or rural areas and at time periods (e.g., different reasons). It will be helpful if the authors can provide any model

performance in terms of spatial pattern (e.g., prediction biases) or time series of observation-simulation comparison. The result can be added in an appendix part if pages are limited.

Thanks for the suggestion. We have already had the statistics and discussions of each individual air quality site shown in Figures 3/4 and section 3.1.2.b. We added the time series of observation-simulation comparison averaged over the areas where the monitoring sites were located in the supplement material as shown in the following figures. We also inserted some discussions in section 3.1.1 for meteorological comparisons and in 3.1.2.a for regional average air quality comparisons.

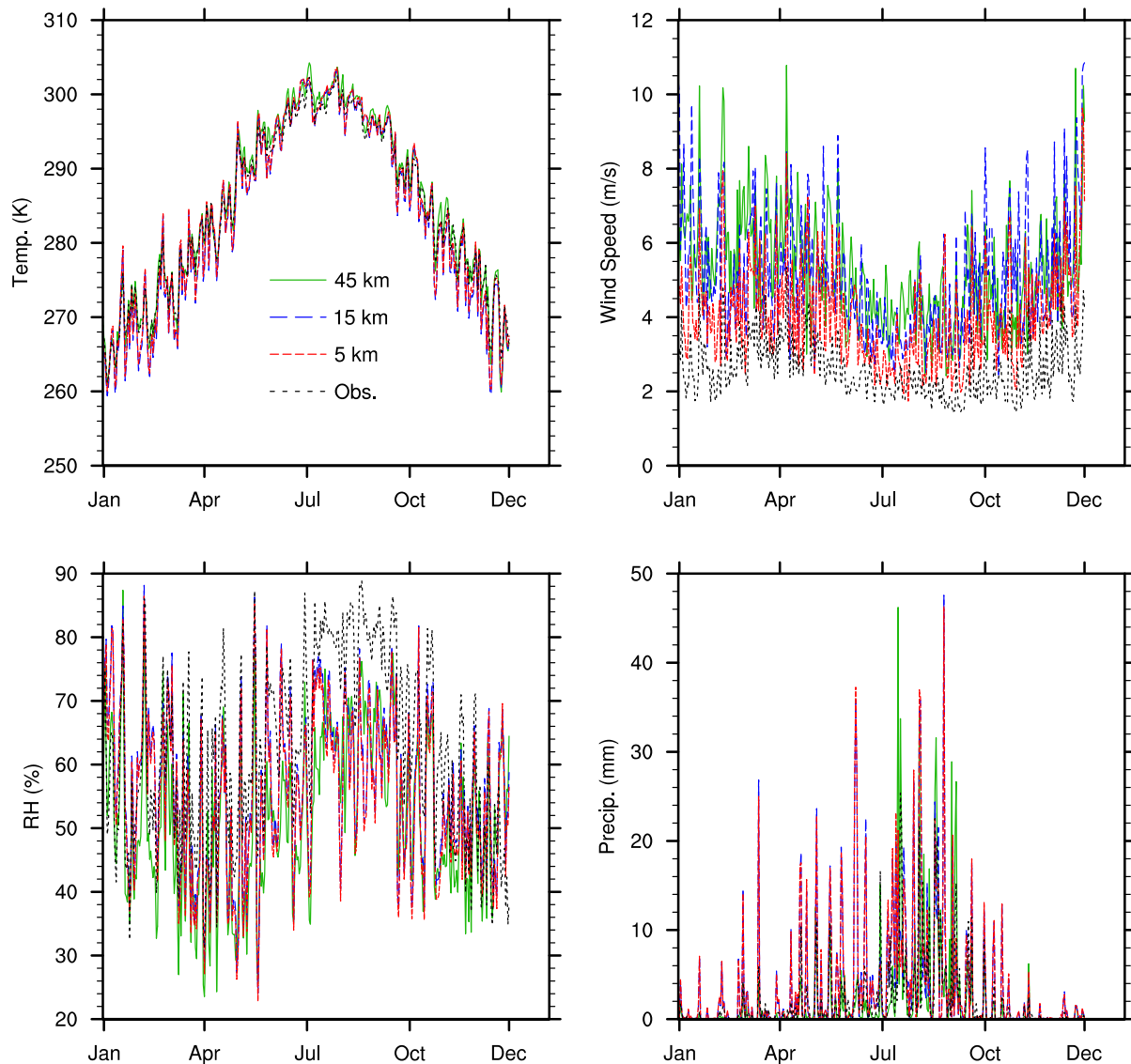


Figure 1s. Time series of surface meteorological parameters of observed vs. modeled values at different grid resolutions in areas where the monitoring sites are located.

At the end of section 3.1.1

“The time series of daily mean wind speed, air temperature, and RH, as well as daily total precipitation averaged over the monitoring sites is illustrated in Figure 1s in the supplement material. It echoed the above findings based on the Taylor diagram. It appeared that NU-WRF constantly overestimated surface wind speed throughout the year with large overestimate occurring in fall and winter, while it severely underestimated RH in summer. Uncertainty in representation of land surface characteristics at least partially explained these biases (Yu, 2014; Gao et al., 2018). High-resolution grid tended to reduce the uncertainty in land surface representation, which would be helpful to improving model performance in meteorology simulation. A more detailed exploration of model-observation mismatch was insightful but beyond the scope of this research.”

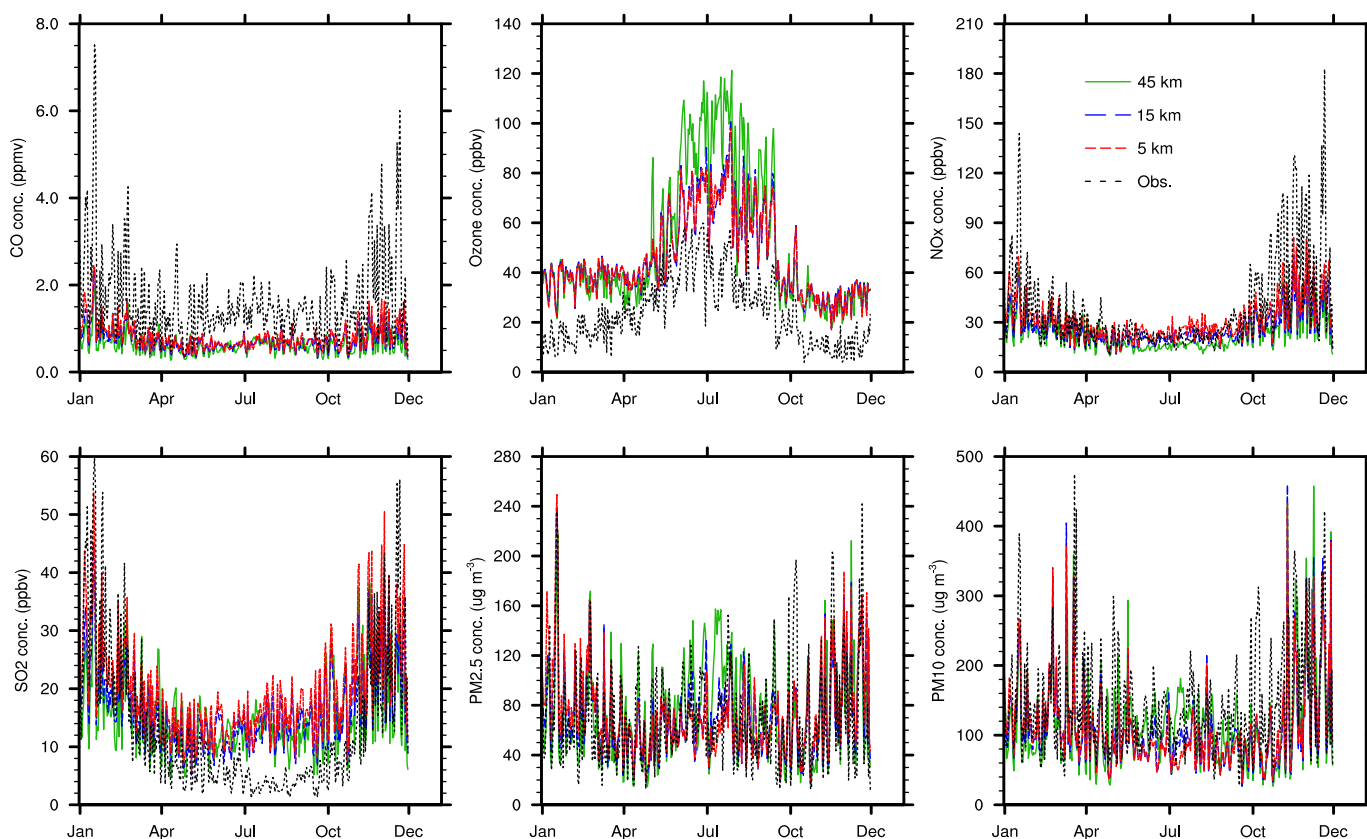


Figure 2s. Time series of surface air quality of observed vs. modeled values at different grid resolutions in areas where the monitoring sites are located.

At the end of section 3.1.2.a

“Figure 2s in the supplement material shows the time series of daily mean air quality averaged over the monitoring sites for the year 2010. The constant underestimate of CO throughout the year, severe underestimate of NOx in fall and winter, and large underestimate of SO₂ in summer all pointed out that the

emissions inventory may be incomplete, agreeing with the reports by Kong et al. (2019) and Li et al. (2019). In the future, improvement of the emissions inventory accuracy and more realistic temporal emissions distribution may help improving NU-WRF performance in simulating O₃ photochemistry.”

4. Figure 7: It seems that simulated O₃ spatial patterns are not matched well with that of its precursors including NO_x simulations and isoprene emissions (see Fig.6) at different grid-spacing. For instance, the simulated surface NO_x concentrations at the grid-spacings of 15-km and 5-km grids look very similar to those at the grid-spacing of 45-km. However, the simulated O₃ concentrations out of the 15-km and 5-km grids are much smaller than those at the grid-spacing of 45-km. More explanations will be helpful to readers for better understanding their relationship and the model performance at varying grid-spacings.

This is a good point. Actually, the other reviewer also raised the similar question. The authors believe, through carefully analysis, that the following two factors play major roles in these results. 1) Ozone photochemistry: ozone is a secondary pollutant formed in the atmosphere in the presence of its precursors such as NO_x and VOCs, as well as solar radiation. Except for limited urban areas, ozone formation is typically limited by the availability of NO_x in the vast rural areas as illustrated in Figure 7. In this case, the 45-km grid tended to distribute NO_x emissions more evenly in the region, effectively decreasing the surface NO_x concentration in urban areas but increasing it over rural areas. The larger average wind speeds out of the 45-km grid (Figure 6 and Table 3) in July further smoothed out NO_x distributions in NCP. This in turn increased the domain average surface O₃ concentration via photochemistry based on the 45-km resolution results. 2) Vertical lifting effect: fine resolution (e.g., 15-km and 5-km) modeling tended to produce stronger updraft than a coarse resolution modeling (e.g., 45-km) as shown in Figure 4s. This finding is consistent with the work by Lee et al. (2018) who account this partly for the aerosol-cloud interaction induced freezing/evaporation-related invigoration mechanism. The strong uplift would bring more surface pollutants such as NO_x into the upper atmosphere, thus further reducing the NO_x availability at ground that limits the surface ozone production but increases its formation in the upper atmosphere (see Figure 8 in the manuscript). In future studies, the measured vertical meteorology and pollutant profiles will be extremely helpful in elucidating the reasons.

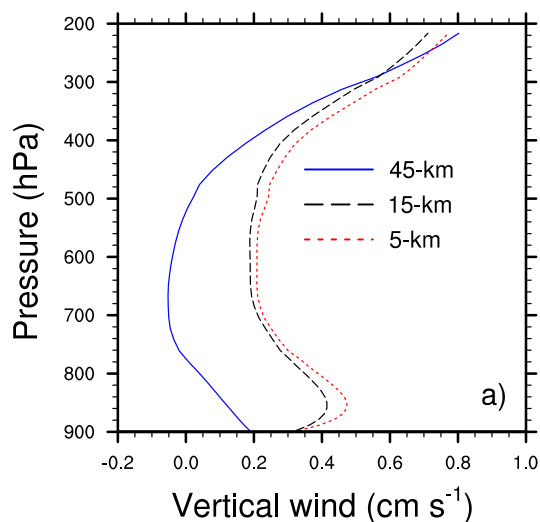


Figure 4s. Domain average vertical wind speed at different grid resolutions along the altitude

A few sentences were added in section 3.2.3:

“...The domain average discussed in this section, however, was the average covering the vast rural area that generally was NO_x-limited such that surface O₃ formation was controlled by the availability of NO_x – more NO_x resulting in more O₃ through photochemical processes. In this case, the 45-km grid tended to distribute NO_x emissions more evenly in the region, effectively decreasing the surface NO_x concentration in urban areas but increasing it over rural areas. The larger average July wind speed simulated by the 45-km grid (Figure 6 and Table 3) further smoothed out the NO_x distribution in NCP. This in turn increased the domain average surface O₃ concentration via photochemistry based on the 45-km resolution results. In addition, vertical lifting played an important role in explaining the maximum regional O₃ in July simulated by the 45-km grid as compared to the results by the other two grid resolutions. As displayed in Figure 4s in the supplement material, a fine resolution modeling (e.g., 5-km) tended to produce a stronger updraft than a coarse resolution modeling (e.g., 45-km), consistent with the findings by Lee et al. (2018). The strong uplift would bring more surface pollutants such as NO_x into the upper atmosphere, thus further reducing the NO_x availability at ground limiting the surface ozone production but increasing its formation in the upper atmosphere.”

5. L430-432: How the maximum PBLH can be observed in Mongolian Plain where surface cover is dominated by grass?

PBL growth is primarily driven by the buoyancy due to surface heating. Thus, PBLH is closely related to the sensible heating at surface. The larger the sensible heating is, the deeper the PBL will be (e.g., Tao et al., 2013). Meanwhile, the high sensible heating is generally associated with a dry soil as reported in Bindlish et al. (2001). Major vegetation coverages over the study domain include grasslands mosaiced with open shrublands (over large portions of the northwest quartile of the domain), croplands (over large portions of eastern part of the domain outside of water), various deciduous forests (areas separate grassland and cropland), and urban. The grassland soil is generally drier than that of other vegetation covers in the domain. This explains why the largest average PBLH is found over the grassland in the northwestern corner of the domain. The text of L432-434 has been modified as:

“...The large average PBLH (more than 1,000 m) was found in the northwestern corner of the domain with a dominant land cover type of grassland mosaiced with open shrubland that appeared to be drier than the other land cover types in the domain. The high sensible heating associated with dry soil tended to produce the deep PBL (Tao et al., 2013).”

6. Table 3: Is it possible to add any available observational data for a comparison? The values presented in Table 3 represent domain average. It is not clear whether the simulations at those grids over ocean were included in the calculations.

The purpose of Table 3 is to facilitate the analysis of inter-resolution model comparison (section 3.2). Therefore, no observational data is listed in this table. The comparisons with the observations have been presented in section 3.1. The regional averages presented in Table 3 were calculated including every grid

(land and ocean) within the domain. We changed the Table title to “[Domain total emissions and average meteorology and air quality at various resolutions](#)”.

7. L60: Is “CHIMERE” defined? Please check similar issue for other abbreviation terms.

CHIMERE is not an abbreviation. It is the name of a Eulerian off-line chemistry-transport model developed in France. We modified the sentence (L61) as “...[using the CHIMERE chemistry-transport model at various horizontal resolutions over Paris](#)”. We also checked the text and spelled out the abbreviation when it first occurred.

8. L120: Is “off” correct?

We modified the sentence to avoid confusion. The new description is “...[new Grell cumulus scheme developed from the ensemble cumulus scheme that allowed subsidence spreading](#)”.

9. L208: “simulated the best precipitation” or “simulated the precipitation best”? I recommend the latter.

We changed the sentence as suggested. We also checked the text to make the recommended changes as appropriate.

Response to Reviewer #2

1. The manuscript concludes that the 15-km resolution model has the overall best performance among the three. This is somewhat surprising as the finest resolution model is often assumed to be better.

In this investigation, we have found that the 5-km resolution modeling provided the best results of wind and surface pollutant levels, especially in polluted conditions that were more relevant to air quality regulation (e.g., compliance of national air quality standards), measured by bias and RMSE. However, the improvement of model performance on air quality was not linear with the resolution increase. For example, the accuracy of modeled surface O₃ out of the 15-km grid was greatly improved over the one from the 45-km grid. Further increase of grid resolution to 5-km, however, showed diminished impact on model performance on O₃ prediction for the study region. In addition, the cost in terms of cpu hours and disk space usage increased dramatically when adopting the 5-km grid resolution, which would be a big hurdle for the inter-model comparison studies such as MICS-Asia that relied on community contributions to model Asian air quality over a relatively long time period. Considering all these factors, we suggest a 15-km resolution grid for future MICS-Asia modeling activity to achieve both accuracy and efficiency. We checked the wording of the manuscript to make it clear that 15-km grid did not provide the best performance but rather was an optimal resolution that balanced the model accuracy and resource usages. For example, we modified the section 4 (Summary) as:

“...With regard to MICS-Asia Phase III whose major goal was to examine regional air quality, in general, the finer the grid resolution was, the better the simulation results would be. This was especially true over the coastal areas and complex terrains where a sharp local energy gradient existed. Fine resolution grid was also extremely helpful to reproducing pollutants at higher concentrations that were most relevant to air quality planning and management. However, the benefit of high resolution was not linear with the decrease of grid size. At certain point, the improved modeling accuracy due to an increase in grid resolution was so marginal that it cannot justify the computational cost associated with the fine grid simulation. Based on the balance of modeling accuracy and efficiency, a 15-km horizontal grid appeared to be an appropriate choice to optimize model performance and resource usage if the study domain remained unchanged for future MICS-Asia activities. The study suggested that the high-resolution emissions, especially the proper representation of emission gradients, would be helpful in improving air quality prediction. Moreover, the profile measurements of both meteorology and air quality, in supplement with the ground monitoring networks, would be greatly helpful to identifying model deficiencies and thus improving model forecast skills.”

2. For the most part, the manuscript provides only domain-mean comparison between the three resolutions against observations. Although site-level model evaluation is shown in the figures, they are mere statistics and lack follow-up investigations or discussions that can be linked to certain model processes or input data that can provide insights for model improvement or can be generalized for other regions and time periods. For example, more analysis should be conducted to examine where/when the variations in meteorology and air quality are the largest within the domain that are most challenging for the 5-km model to capture.

This is a very good suggestion. We went back to data and made more analysis. Based on the results, we believe that the following factors account at least partially for the discrepancy between the modeled and observed air quality. 1) Spatial distribution of emissions was one key to determining air quality forecast accuracy. Out of 25 air quality monitoring sites used for model evaluation, 3 were rural sites and the remaining were urban/suburban sites. Figure 3s shows the typical time evolutions of surface ozone and NO_x over the rural (XL) and urban (QHD) sites. It can readily be seen that NO_x was underestimated at the urban site but overestimated at the rural site. The coarser the grid resolution, the severer the underestimates/overestimates were. This indicated that the 45-km resolution tended to smooth out emissions to make urban (or emissions centers) less polluted but rural more polluted. It in turn led to an overestimate of surface ozone over the urban sites mainly due to the reduced NO_x titration effect, especially at night when there was no photochemical ozone formation. The statistics showed that the bias of the modeled daytime (7 am ~ 7 pm local time) average surface O₃ was 30% ~ 90% smaller than that of the daily average in the urban sites, no matter which grid resolution was applied. This suggests that, in the future, the high-resolution emissions, especially proper representation of emission gradients, will be helpful in improving air quality prediction. This point will be revisited in addressing comment 3.

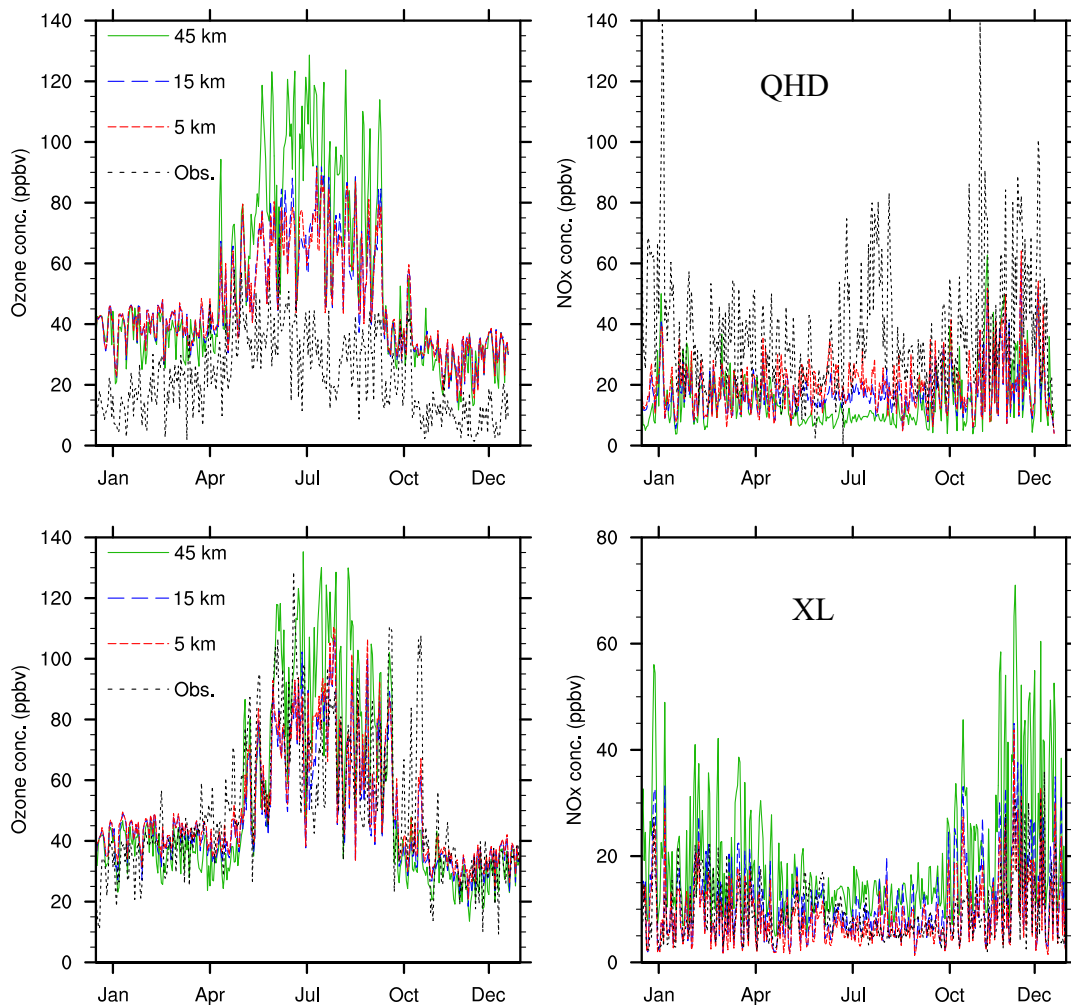
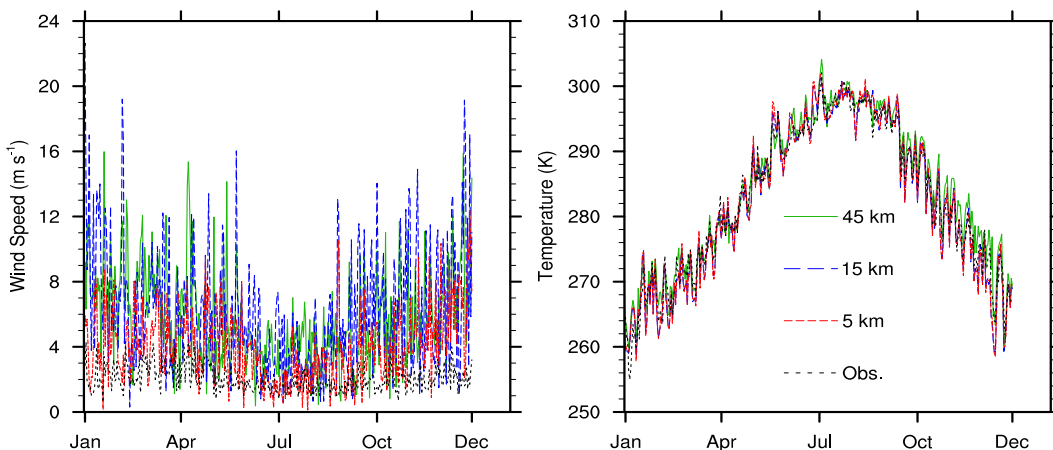


Figure 3s. Time series of surface O₃ and NO_x concentrations over QHD (upper) and XL (lower) sites of the observed vs. modeled values at different grid resolutions.

2) The driving meteorology, especially wind, was important to accurately forecast air quality. Take QHD site as an example. QHD site locates approximately 5 km from the ocean and is subject to sea breeze effects. There is a meteorological monitoring station co-locating at QHD. The temporal profiles of surface wind speed and temperature from the observation and model results out of 3 grids for QHD are shown in the following figure. The results indicated that the choice of grid resolution had large impacts on model simulations at this coastal site. The selection of the 5-km grid reduced biases of both surface temperature and wind speed. The biases of temperature reduced from 1.22 K (45-km) to -0.42 K (15-km), and further down to -0.31 K when the 5-km grid was applied. The biases of surface wind speed for the 45-km, 15-km, and 5-km grids were 3.72, 4.19, and 1.95 m s⁻¹, respectively. The improvement of meteorology forecast helped reducing the biases of air quality modeling. The biases of ozone/NO_x for the 45-km, 15-km, and 5-km resolution grids were 29.94/-22.46 ppbv, 24.09/-20.29 ppbv, 23.97/-17.95 ppbv, respectively. The improvement using the 15-km grid over the 45-km grid was remarkable but that using the 5-km grid over the 15-km grid was marginal. Vertical wind profile was another important factor to determine surface air quality as shown in the answer to Comment 4. This emphasizes the importance to measure vertical profiles of both meteorology and air quality in the future, which will help improve model skills.



3) Photochemistry mechanism also impacts the model performance. This has been shown in the companion papers by Li et al. (2019) and Kong et al. (2019).

In summary, the authors find out that a high-resolution emissions inventory would greatly help improving the model performances, especially over urban areas and emissions centers. Over the coastal areas (e.g., QHD) and complex terrain areas (e.g., XL), high resolution modeling tends to produce a more realistic wind field that benefits air quality simulation. In the future, the profile measurements of both meteorology and air quality are needed to elucidate the discrepancy between simulation and observation, thus help to improve model skills. We added discussions in section 3.1.2.b (Individual site), section 3.2.3 (see answer to Comment 4), and section 4 (see answer to Comment 1) to reflect the above analysis.

In section 3.1.2.b:

“An effort has been put to identify the potential reasons that caused the model-observation discrepancy. First and as discussed previously, the spatial distribution of emissions was one key to determining air quality forecast accuracy. Figure 3s shows the typical time evolutions of surface O₃ and NO_x over the rural (XL) and urban (QHD) sites. It can readily be seen that NO_x was underestimated at the urban site but overestimated at the rural site. The coarser the grid resolution, the severer the underestimates/overestimates were. This indicated that the 45-km resolution tended to smooth out emissions to make urban (or emissions centers) less polluted but rural more polluted. It in turn led to an overestimate of surface O₃ over the urban sites mainly due to the reduced NO_x titration effect, especially at night when there was no photochemical O₃ formation. The statistics showed that the bias of the modeled daytime (7 am ~ 7 pm local time) average surface O₃ was 30% ~ 90% smaller than that of the daily average in the urban sites, no matter which grid resolution was applied. This suggested that in the future the high-resolution emissions, especially proper representation of emission gradients, would be helpful in improving air quality prediction. The effect of emissions gradients associated with the grid resolution would be further discussed in the inter-model comparison section.

Next, the driving meteorology, especially wind, was important to accurately forecast air quality over coastal areas that bore sharp thermal contrasts. QHD site locates approximately 5 km from the ocean and is subject to sea breeze effects. The detailed analysis of meteorology and air quality over QHD was conducted. The results indicated that the choice of grid resolution had large impacts on model simulations at this coastal site. The selection of the 5-km grid reduced biases of both surface temperature and wind speed. The biases of temperature reduced from 1.22 K (45-km) to -0.42 K (15-km), and further down to -0.31 K when the 5-km grid was applied. The biases of surface wind speed for the 45-km, 15-km, and 5-km grids were 3.72, 4.19, and 1.95 m s⁻¹, respectively. The improvement of meteorology forecast helped reducing the biases of air quality modeling. The biases of O₃/NO_x for the 45-km, 15-km, and 5-km resolution grids were 29.94/-22.46 ppbv, 24.09/-20.29 ppbv, 23.97/-17.95 ppbv, respectively. The improvement using the 15-km grid over the 45-km grid was remarkable but that using the 5-km grid over the 15-km grid was marginal. The result emphasized the importance of high-resolution modeling to improvements of air quality forecast skills, especially at coastal and complex terrain areas (e.g., QHD and XL).”

3. It is not clear whether the model input data are resolution aware. Are the underlying emissions inventory data and land surface data (topography, LAI, etc) at a fine resolution of 5 km and then aggregated to the coarser resolutions? If the model is not driven by inputs that can resolve 5-km surface conditions, the 5-km model will not be able to correctly simulate air pollution variations at the 5-km scale.

Thanks for raising a very important point. In addition to the computation constrain, the challenge to employing an ultra-fine resolution modeling is the availability of the input data that are at the same or similar resolution. In this study, the land surface data were derived from the 30s resolution (around 30 m along mid-latitude) MODIS products that were aggregate to the model resolution. However, the MIX anthropogenic and GFEDv3 fire emissions inventories utilized in the study have a resolution of 0.25 by 0.25 degree and 0.5 by 0.5 degree, respectively. As indicated in the answer to Comment 2 above, the uncertainty of emissions may lead to air quality modeling errors. Therefore, the resolution-aware emissions may further improve the model performance using a 5-km grid. We added a caveat in section 4 (Summary) to reflect this.

“... It also was worth noting that the benefit of increasing grid resolution to better surface O₃ and PM_{2.5} simulations started to diminish when the horizontal resolution reached 15-km, agreeing with the finding by Valari and Menut (2008). There is a caveat, though. The anthropogenic MIX and fire GFEDv3 emissions inventories bore the 0.25° by 0.25° and 0.5° by 0.5° resolution, respectively. These resolutions cannot resolve the 5-km grid. Should a 5-km resolution emissions inventory be available and used, the benefit of high-resolution modeling would likely be more prominent.”

4. Figure 7, top panel: Ozone simulated by the 45-km model is almost 20 ppbv higher than the other two resolutions for July throughout the whole domain, while emissions of ozone precursors and meteorology are not so different. Why? Is this some kind of model error? If the model’s oxidant budget is strongly resolution-dependent, one will question whether the model processes are parameterized correctly. A stable model should produce regional-mean concentrations of key species that are more or less consistent between different resolutions; it is the sub-regional variability and extreme concentrations that will differ as the resolution changes. This is reflected in ozone simulated by the 15-km and 5-km grids, but the 45-km model is an outlier.

Thanks for pointing this out. Actually, the first reviewer also raised the similar question. The authors believe, through carefully analysis, that the following two factors play major roles in these results. 1) Ozone photochemistry: ozone is a secondary pollutant formed in the atmospheric in the presence of its precursors such as NO_x and VOCs, as well as solar radiation. Except for limited urban areas, ozone formation is typically limited by the availability of NO_x in the vast rural areas as illustrated in Figure 7. In this case, the 45-km grid tended to distribute NO_x emissions more evenly in the region, effectively decreasing the surface NO_x concentration in urban areas but increasing it over rural areas. The larger average wind speeds out of the 45-km grid (Figure 6 and Table 3) in July further smoothed out NO_x distributions in NCP. This in turn increased the domain average surface O₃ concentration via photochemistry based on the 45-km resolution results. Actually, the spatial distributions of annual average surface O₃ out of three grids appeared to be less variable. 2) Vertical lifting effect: fine resolution (e.g., 15-km and 5-km) modeling tended to produce a stronger updraft than a coarse resolution modeling (e.g., 45-km) as shown in Figure 4s. This finding is consistent with the work by Lee et al. (2018) who account this partly for the aerosol-cloud interaction induced freezing/evaporation-related invigoration mechanism. The strong uplift would bring more surface pollutants such as NO_x into the upper atmosphere, thus further reducing the NO_x availability at ground that limits the surface ozone production but increases its formation in the upper atmosphere (see Figure 8 in the manuscript). In future studies, the measured vertical meteorology and pollutant profiles will be extremely helpful in elucidating the reasons.

A few sentences were added in section 3.2.3:

“...The domain average discussed in this section, however, was the average covering the vast rural area that generally was NO_x-limited such that surface O₃ formation was controlled by the availability of NO_x – more NO_x resulting in more O₃ through photochemical processes. In this case, the 45-km grid tended to distribute NO_x emissions more evenly in the region, effectively decreasing the surface NO_x concentration in urban areas but increasing it over rural areas. The larger average July wind speed simulated by the 45-km grid (Figure 6 and Table 3) further smoothed out the NO_x distribution in NCP. This in turn increased the domain average surface O₃ concentration via photochemistry based on the 45-km resolution results. In addition, vertical lifting

played an important role in explaining the maximum regional O₃ in July simulated by the 45-km grid as compared to the results by the other two grid resolutions. As displayed in Figure 4s in the supplement material, a fine resolution modeling (e.g., 5-km) tended to produce a stronger updraft than a coarse resolution modeling (e.g., 45-km), consistent with the findings by Lee et al. (2018). The strong uplift would bring more surface pollutants such as NO_x into the upper atmosphere, thus further reducing the NO_x availability at ground limiting the surface ozone production but increasing its formation in the upper atmosphere.”

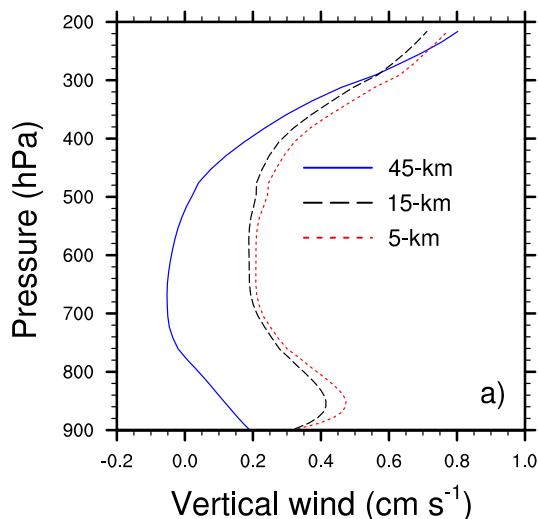


Figure 4s. Domain average vertical wind speed at different grid resolutions along the altitude

5. Table 3: Natural emissions (isoprene, dust, and sea salt) are very different between the three resolutions, varying by almost a factor of two. While these emissions are dependent on meteorology and thus on the model resolution, the standard practice is to implement a scaling factor so that the domain-wide emissions are consistent between different resolutions. Otherwise, it will not be a fair comparison as the emissions are not constant across the three resolutions. As this manuscript is part of a model intercomparison study, these emissions should be consistent with other models participating in the study.

We treated the biogenic, dust, and seasalt emissions that were calculated online as part of the effect of grid resolutions on air quality since the meteorological driving forces of these emissions, such as temperature, solar radiation, and wind, were impacted by the choice of grid resolutions. We think this is a fair justification.

6. Line 215-210: the different conclusion from Gao et al. was due to the difference in observations or in the model setting?

Gao et al. investigated the grid resolution effect on precipitation over the contiguous U.S. Their domain, modeling setup, and observations were all different from the ones used in this study. More

importantly, Gao et al. used the processed precipitation data for their model evaluation – their precipitation data were based on the daily rain gauge data that were gridded to the 0.125° resolution using the synergraphic mapping algorithm with topographic adjustment to the monthly precipitation climatology. The processed data promoted the precipitation homogeneity and reduced the chances of model-observation mismatch of a precipitation event. This may be the major reason that two studies draw the opposite conclusions. In the manuscript we emphasized that our conclusion was based on the comparison with the site observation. For example, in section 4 (Summary):

“...The statement on precipitation should be taken with caution since it was based on the comparison with the site observations. Seeing the very heterogeneous nature of precipitation, the penalty of model hitting or missing a rain event was severe. Thus, the coarse grid covering more areas within a grid cell would reduce chances of mistaken precipitation hitting or missing simulations. However, a comparison of modeled precipitations to gridded “observation” that was re-constructed using the synergraphic mapping algorithm with topographic adjustment to the monthly precipitation climatology showed opposite result, where the fine resolution modeling showed superior reproduction of precipitation than the coarse resolution simulation (Gao et al., 2017).”

7. Table 2: I don’t understand this table. What are the numbers in each cell and why they are so different?

Table 2 lists the occurrences of exceedances of China’s National Ambient Air Quality Standards (NAAQS). Column “Frequency” indicates the time integration of each NAAQS. Column “Class 1” lists the NAAQS for rural sites, and “Class 2” lists the standards for urban-suburban sites. “Obs” lists the occurrences of NAAQS exceedances for each pollutant based on the observations. Columns “45-km”, “15-km”, and “5-km” list the occurrences of NAAQS exceedances based on the modeling results using “45-km”, “15-km”, and “5-km” grid resolutions. We added a sentence in section 3.1.2.c:

“Table 2 lists the occurrences of violations of China’s national ambient air quality standards (NAAQS) for the six pollutants from both observations and simulations, in which columns “Class 1” and “Class 2” list the standards for rural and urban-suburban sites, respectively, and column “Frequency” indicates the time integration of each NAAQS.”

8. Line 32: add “the” before 21st century.

Done.

9. Line 68: remove “however”.

Done.

Evaluation of NU-WRF Performance on Air Quality Simulation under Various Model Resolutions – An Investigation within Framework of MICS-Asia Phase III

Zhining Tao^{1,2}, Mian Chin², Meng Gao³, Tom Kucsera^{1,2}, Dongchul Kim^{1,2}, Huisheng Bian^{2,4}, Jun-ichi Kurokawa⁵, Yuesi Wang⁶, [Zirui Liu⁶](#), Gregory R. Carmichael⁷, Zifa Wang^{6,8,9}, and Hajime Akimoto¹⁰

Formatted: Superscript

1. Universities Space Research Association, Columbia, MD, USA
2. NASA Goddard Space Flight Center, Greenbelt, MD, USA
3. John A. Paulson School of Engineering and Applied Sciences, Harvard University, Cambridge, MA, USA
4. University of Maryland at Baltimore County, Baltimore, MD, USA
5. Japan Environmental Sanitation Center, Asia Center for Air Pollution Research, Niigata, 950-2144, Japan
6. State Key Laboratory of Atmospheric Boundary Layer Physics and Atmospheric Chemistry, Institute of Atmospheric Physics, Chinese Academy of Sciences, Beijing, 100029, China
7. Center for Global and Regional Environmental Research, University of Iowa, Iowa City, IA, USA
8. College of Earth Sciences, University of Chinese Academy of Sciences, Beijing, 100049, China
9. Center for Excellence in Urban Atmospheric Environment, Institute of Urban Environment, Chinese Academy of Sciences, Xiamen, 361021, China
10. National Institute for Environmental Studies, Onogawa, Tsukuba, 305-8506, Japan

1 **Abstract**

2
3 Horizontal grid resolution has a profound effect on model performances on meteorology
4 and air quality simulations. In contribution to MICS-Asia Phase III, one of whose goals was to
5 identify and reduce model uncertainty in air quality prediction, this study examined the impact of
6 grid resolution on meteorology and air quality over East Asia, focusing on the North China Plain
7 (NCP) region. NASA Unified Weather Research and Forecasting (NU-WRF) model has been
8 applied with the horizontal resolutions at 45-, 15-, and 5-km. The results revealed that, in
9 comparison with ground observations, no single resolution can yield the best model performance
10 for all variables across all stations. From a regional average perspective (i.e., across all monitoring
11 sites), air temperature modeling was not sensitive to the grid resolution but wind and precipitation
12 simulation showed the opposite. NU-WRF with the 5-km grid simulated the wind speed **best**, while
13 the 45-km grid yielded the most realistic precipitation as compared to the site observations. For air
14 quality simulations, finer resolution generally led to better comparisons with observations for O₃,
15 CO, NO_x, and PM_{2.5}. However, the improvement of model performance on air quality was not
16 linear with the resolution increase. The accuracy of modeled surface O₃ out of the 15-km grid was
17 greatly improved over the one from the 45-km grid. Further increase of grid resolution **to 5-km**,
18 however, showed diminished impact on model performance **improvement** on O₃ prediction. In
19 addition, **5-km** resolution grid showed large advantage to better capture the frequency of high
20 pollution occurrences. This was important for assessment of noncompliance of ambient air quality
21 standards, which was key to air quality planning and management. Balancing the **modeling**
22 **accuracy** and resource limitation, a 15-km grid resolution was suggested for future MICS-Asia air
23 quality modeling activity **if the research region remained unchanged**. This investigation also found
24 out large overestimate of ground-level O₃ and underestimate of surface NO_x and CO, likely due
25 to missing emissions of NO_x and CO.
26
27

Deleted: best

Deleted: finer

Deleted: findings

31 **1. Introduction**

32 Air pollution is a threat to human health/climate and detrimental to ecosystem (Anenberg
33 et al., 2010; <https://www.who.int/airpollution/ambient/en/>). Lelieveld et al. (2015) estimated that
34 over 3 million premature mortality could be attributable to outdoor air pollution worldwide in 2010
35 based on their analysis of data and the results from a high-resolution global air quality model.
36 Since the turn of [the 21st century](#), East Asia has undergone remarkable changes in air quality as
37 observed by satellite and ground stations (Jin et al., 2016; Krotkov et al., 2016). In the past decade,
38 haze (fine particle) pollution has become a household name in China and many severe haze events
39 have been reported and their formation mechanisms and associations with global- and meso-scale
40 meteorology have been analyzed (Zhao et al., 2013; Huang et al., 2014; Gao et al., 2016; Cai et
41 al., 2017; Zou et al., 2017). Meanwhile, ground level ozone has been a major air quality concern
42 in China (Wang et al., 2017; Lu et al., 2018), Japan (Akimoto et al., 2015), and South Korea (Seo
43 et al., 2014). In combination with observations from various platforms, chemical transport model
44 (CTM) remains an important tool to understand mechanisms, to investigate spatial-temporal
45 distributions, and to design feasible control strategies of air pollution. However, CTM model
46 uncertainties persist (e.g., Carmichael et al., 2008) and the interpretation of any model results needs
47 caution and exertion of careful analysis.

48 Inter-model comparison study provides a valuable way to understand model uncertainties
49 and sheds light on model improvements. With this as one of its major goals, the Model Inter-
50 Comparison Study for Asia (MICS-Asia) was initiated in 1998. Since then MICS-Asia has gone
51 through three phases with emphasis on various aspects of air pollution. Phase I focused on long-
52 range transport and deposition of sulfur over East Asia (Carmichael et al., 2002). Phase II expanded
53 the analysis on more pollutants including nitrogen compounds, particulate matter, and ozone, in
54 addition to sulfur (Carmichael et al., 2008). Fast moving to Phase III, MICS-Asia concentrated on
55 three topics with number one aiming at identifying strengths and weaknesses of current air quality
56 models to provide insights on reducing uncertainties (Gao et al., 2018). There are totally 14 CTMs
57 – 13 regional and 1 global – participating in the coordinated model experiment, which simulated
58 air quality over Asia throughout the year 2010. Due to the constrain of computing resources among
59 participating modeling groups, a 45-km horizontal resolution has been commanded for every team
60 to run the year-long experiment.

61 This relatively coarse spatial resolution raises the question of how representative the model
62 can resolve key issues relevant to air quality and its planning/regulation, e.g., heterogeneous
63 emissions, inhomogeneous land cover and meteorology. For example, Valari and Menut (2008)
64 explored the issue using the CHIMERE [chemistry-transport](#) model at various horizontal
65 resolutions over Paris. They found out that the ozone simulation was especially sensitive to the
66 resolution of emissions. However, the benefit of increasing emissions resolutions to improve ozone
67 forecast skills was not monotonic and at certain point the forecast accuracy decreased upon further
68 resolution increase. Using the Weather Research and Forecasting Chemistry model (WRF-Chem)
69 with various horizontal resolution (3 ~ 24 km) over the Mexico City, Tie et al. (2010) concluded
70 that a 1 to 6 ratio of grid resolution to city size appeared to be a threshold to improve ozone
71 forecasting skill over mega-city areas: the forecast would be improved significantly when model
72 resolution was below this threshold value. On contrary to Valari and Menut (2008), Tie et al. (2010)
73 suggested that the meteorology changes associated with the grid size choice played a more
74 prominent role in contributing to the improvement of ozone forecast skills. More recently, Neal et
75 al. (2017) employed a high-resolution (12 km) air quality model with high-resolution emissions
76 within the Met Office's Unified Model (AQU) for air quality forecast over the Great Britain.

Deleted: however,

78 They found out that AQUM significantly improved the forecast accuracy of primary pollutants
79 (e.g., NO₂ and SO₂) but less obviously for secondary pollutants like ozone, as compared with a
80 regional composition-climate model (RCCM, 50 km horizontal resolution). But there was a
81 drawback from their conclusion in that the chemical mechanisms and photolysis rates utilized in
82 AQUM and RCCM were different, complicating the underlying reasons for changes in forecast
83 skills. Lee et al. (2018) examined the importance of aerosol-cloud-radiation interactions to
84 precipitation and the model resolution impact of key meteorological processes that affected
85 precipitation using the Advanced Research WRF model. They found that the coarse model
86 resolution would lower updraft, alter cloud properties (e.g. mass, condensation, evaporation, and
87 deposition), and reduce cloud sensitivity to ambient aerosol changes. They further concluded that
88 the uncertainty associated with resolution was much more than that related to cloud microphysics
89 parameterization. The resultant meteorological condition change would trigger air quality response
90 as well.

91 Despite the progress, the exploration of impacts of model resolution on local air quality
92 over Asia is rare. Taking advantage of the MICS-Asia platform, we examined the issue over the
93 MICS-Asia domain using the NASA Unified WRF (NU-WRF, Tao et al., 2013, 2016, 2018;
94 Peters-Lidard et al., 2015), focusing on the North China Plain (NCP) that was plagued by frequent
95 heavy air pollution episodes. The investigation would not only assist in gaining insights on how
96 model horizontal resolution affects simulated meteorology and air quality, but also contribute to
97 formulation of uncertainties resulted from model resolutions to the MICS-Asia community. The
98 latter would especially be valuable since most MICS-Asia Phase III model simulations were
99 conducted at a specific horizontal resolution (i.e., 45-km for most participants).

100

101 2. NU-WRF model and experiment design

102 NU-WRF is an integrated regional Earth-system modeling system developed from the
103 advanced research version of WRF-Chem (Grell et al., 2005), which represents atmospheric
104 chemistry, aerosol, cloud, precipitation, and land processes at convection-permitting spatial scales
105 (typically 1-6 km). NU-WRF couples the community WRF-Chem with NASA's Land Information
106 System (LIS), a software framework including a suite of land surface models (LSMs) that are
107 driven by satellite/ground observations and reanalysis data (Kumar et al., 2006; Peters-Lidard et
108 al., 2007). It also couples the Goddard Chemistry Aerosol Radiation and Transport (GOCART)
109 bulk aerosol scheme (Chin et al., 2002, 2007) with the Goddard radiation (Chou and Suarez, 1999)
110 and microphysics schemes (Tao et al., 2011; Shi et al., 2014) that allows for fully coupled aerosol-
111 cloud-radiation interaction simulations. In addition, NU-WRF links to the Goddard Satellite Data
112 Simulator Unit (G-SDSU), which converts simulated atmospheric profiles, e.g. clouds,
113 precipitation, and aerosols, into radiance or backscatter signals that can directly be compared with
114 satellite level-1 measurements at a relevant spatial and temporal scale (Matsui et al., 2009, 2013,
115 2014). In this study, NU-WRF has been employed to carry out the model simulations at various
116 horizontal resolutions using the same set of physical and chemical configurations.

117 A nested domain setup was configured to this investigation as shown Figure 1. The 45-km
118 resolution mother domain (d01) covered the MICS-Asia Phase III study region. The nested 15-km
119 (d02) and 5-km (d03) domains covered the East Asia and NCP, respectively. A one-way nesting
120 approach was applied so that the values of the mother domains were independent on those of the
121 respective nested domains. This analysis focused on NCP and its adjacent areas with over 1.1
122 million square kilometers. The key NU-WRF configurations included the updated Goddard
123 cumulus ensemble microphysics scheme (Tao et al., 2011), new Goddard long/shortwave radiation

124 scheme (Chou and Soares, 1999), Monin-Obukhov surface layer scheme, unified Noah land
 125 surface model (Ek et al., 2003) with LIS initialization (Peters-Lidard et al., 2015), Yonsei
 126 University planetary boundary layer scheme (YSU, Hong et al., 2006), new Grell cumulus scheme
 127 developed from the ensemble cumulus scheme (Grell and Devenyi, 2002) that allowed subsidence
 128 spreading (Lin et al., 2010), 2nd generation regional acid deposition model (RADM2, Stockwell et
 129 al., 1990; Gross and Stockwell, 2003) for trace gases and GOCART for aerosols. In this
 130 investigation, the option of fully coupled GOCART-Goddard microphysics and radiation schemes
 131 (Shi et al., 2014) has been implemented to account for the aerosol-cloud-radiation interactions.

132 Anthropogenic emissions were from the mosaic Asian anthropogenic emissions inventory
 133 (MIX, Li et al., 2017) that was developed for the MICS-Asia Phase III. The MIX inventory was at
 134 the 0.25° by 0.25° resolution and projected to the study domain under the 45-, 15-, and 5-km
 135 horizontal resolutions. Fire emissions were from the 0.5° by 0.5° Global Fire Emissions Database
 136 version 3 (GFEDv3, van der Werf et al., 2010; Mu et al., 2011) and also projected to the targeted
 137 region. Biogenic emissions were computed online using the Model of Emissions of Gases and
 138 Aerosols from Nature version 2 (MEGAN2, Guenther et al., 2006). Dust and sea salt emissions
 139 were also calculated online using the dynamic GOCART dust emissions scheme (Kim et al., 2017)
 140 and sea salt scheme (Gong, 2003), respectively.

141 The meteorological Lateral Boundary Conditions (LBCs) were derived from the Modern
 142 Era Retrospective-Analysis for Research and Applications (MERRA, Rienecker et al., 2011). The
 143 trace gas LBCs were based on the 6-hour results from the Model for Ozone And Related chemical
 144 Tracers (MOZART, Emmons et al., 2010). The aerosol LBCs were from the global GOCART
 145 simulation with a resolution of 1.25 (longitude) by 1 (latitude) degree (Chin et al., 2007). Three
 146 horizontal resolutions varied from 45-km to 5-km with 15-km in between. Terrain-following sixty
 147 vertical levels stretched from surface to 20 hPa with the 1st layer height of approximately 40 meters
 148 from surface. The simulation started on December 20, 2009, and ended on December 31, 2010,
 149 with the first 11 days as the spin-up.

151 3. Results

152 3.1. Comparisons with observations

153 The NU-WRF results out of different horizontal resolutions have compared with ground
 154 observations using the following statistic measures:

155	Correlation coefficient:	$r = \frac{\sum_{i=1}^n (m_i - \bar{m})(o_i - \bar{o})}{\sqrt{\sum_{i=1}^n (m_i - \bar{m})^2} \sqrt{\sum_{i=1}^n (o_i - \bar{o})^2}}$
156	Mean bias:	$MB = \frac{1}{n} \sum_{i=1}^n (m_i - o_i)$
157	Normalized mean bias:	$NMB = \frac{\sum_{i=1}^n (m_i - o_i)}{\sum_{i=1}^n o_i} \times 100\%$
158	Root mean square error:	$RMSE = \sqrt{\frac{\sum_{i=1}^n (m_i - o_i)^2}{n}}$
159	Normalized standard deviation:	$NSD = \frac{\sqrt{\frac{\sum_{i=1}^n (m_i - \bar{m})^2}{n-1}}}{\sqrt{\frac{\sum_{i=1}^n (o_i - \bar{o})^2}{n-1}}}$

160 Where, m_i and o_i denote for the modeled and observed values at time-space pair i ; \bar{m} and \bar{o}
 161 represent the average modeled and observed values, respectively. r describes the strength and
 162 direction of a linear relationship between two variables – a perfect correlation has a value of 1.
 163 NMB and MB depict the mean deviation of modeled results from the respective observations. A

Deleted: off

165 perfect model simulation yields an *NMB* and a *MB* of 0. *RMSE* measures the absolute accuracy of
166 a model prediction. The smaller the *RMSE*, the better the model performance is. Similar to *NMB*
167 and *MB*, a *RMSE* of 0 indicates a perfect model prediction. *NSD* is a measure to check how well
168 the model can reproduce the variations of observations – a value of 1 represents a perfect
169 reproduction of observed variations.

170

171 3.1.1. Meteorology

172 The 2010 meteorological observations were collected at the standard stations operated by
173 China Meteorological Administration (CMA, <http://data.cma.cn/en>). The locations of each site
174 within our study domain were represented with the black dots in Figure 1. In total there were 77
175 sites reporting daily average values of wind speed (Wind), air temperature (Temp), and relative
176 humidity (RH), as well as daily total precipitation (Precip). Figure 2 (top row) shows the Taylor
177 diagram summarizing *r*, *NMB*, and *NSD* of the comparison of regional mean (average of
178 observations from 77 sites) daily meteorological variables. Along the azimuthal angle is *r*. *NSD*
179 is proportional to the radial distance from the origin. *NMB* (sign and range) are represented by
180 geometric shapes. The statistical measures under 45-, 15-, and 5-km resolutions are represented by
181 color blue, green, and red, respectively. The closer to the point “Obs” on the Taylor diagram and
182 smaller of *NMB*, the better the model performance is.

183 It can be seen that the model horizontal resolution has little impact on surface air
184 temperature simulation. Regardless of resolution selections, the modeled temperature correlated
185 very well with the corresponding observations with *r* values all approaching 0.99. NU-WRF also
186 reproduced the observed temperature variations well with *NSD* ranging between 1.05 and 1.10.
187 Meanwhile, *NMB* was within $\pm 1\%$ for all experimented resolutions. *RMSEs* were 1.13 K, 2.26 K,
188 and 2.02 K for the 45-km, 15-km, and 5-km grids, respectively. The insensitivity of surface air
189 temperature to the choice of model resolutions was also reported by Gao et al. (2017), who used
190 WRF to explore the issue for summer seasons at the 36-, 12-, and 4-km resolutions.

191 On the other hand, the horizontal resolution has a remarkable effect on surface wind speed
192 as shown in Figure 2 (top row). At 5-km resolution, NU-WRF yielded a *r* value of 0.75, *NMB* of
193 approximately 54%, and *NSD* of 1.78. NU-WRF simulated a large variation in wind than the
194 observed ones. As comparisons, the values of *r*, *NMB*, and *NSD* for 15-km and 45-km were 0.54,
195 95%, 2.14, and 0.71, 103%, 2.01, respectively. The respective *RMSEs* out of the 45-km, 15-km,
196 and 5-km grids were 2.87, 2.82, and 1.67 m s⁻¹. It was apparent that 5-km resolution gave the
197 overall best wind speed simulation compared to the observations, though NU-WRF overestimated
198 the surface wind speed in all cases. The wind speed overestimate, especially under low wind
199 conditions, was a common problem in all MICS-Asia participating models and other weather
200 forecast models (Gao et al., 2018). This overestimate stemmed from many factors, including but
201 not limited to terrain data uncertainty, poor representation of urban surface effect, horizontal and
202 vertical grid resolutions, etc. Dr. Yu (2014) in her doctoral dissertation pointed out that surface
203 wind simulation would be improved upon using more accurate land-use data. This is expected
204 since surface wind is largely dependent on the land surface characteristics, such as albedo and
205 roughness. High-resolution grid tends to have more accurate land-use representation seeing the
206 inhomogeneous nature of land type.

207 NU-WRF simulations at all three resolutions yielded the similar reproductions of the
208 observed variations in relative humidity (RH) with the *NSD* ranging between 0.87 and 0.88. The
209 modeled RH was less variable than the observed one. While the modeled RH at 45-km resolution
210 (*r* = 0.84) better correlated with the observations than those at the finer resolutions did

211 (approximately 0.67 for both 15-km and 5-km resolutions), the *NMB* at this resolution was the
212 largest (-17%) among the three cases. The *NMBs* for 15-km and 5-km cases were -10% and -12%,
213 respectively. Overall, NU-WRF underestimated the surface RH. The respective *RMSEs* for 45-km,
214 15-km, and 5-km resolutions were 13.2%, 12.6%, and 13.3%. The simulation with the 15-km grid
215 appeared to yield the overall best RH in three cases.

216 It was interesting to find that NU-WRF simulated the precipitation best, as directly
217 compared to the rain gauge data, when using the 45-km grid. At this resolution, NU-WRF gave *r*
218 of 0.81, *NMB* of 1.7%, *RMSE* of 3.2 mm day⁻¹, and *NSD* of 1.41. As comparisons, the values of *r*,
219 *NMB*, *RMSE*, and *NSD* for 15-km and 5-km were 0.53, 76%, 5.7 mm day⁻¹, 1.71, and 0.52, 80%,
220 5.8 mm day⁻¹, 1.72, respectively. Finer resolutions indeed yielded worse results in precipitation
221 modeling as compared to the site data. This may be because precipitation was a very heterogeneous
222 phenomenon – finer model grid had larger chances to miss a precipitation event or hit an event
223 that was not existent, leading to greater overall bias and poorer correlation. On the contrary, Gao
224 et al. (2017) compared their WRF modeled results to the gridded precipitation based on daily rain
225 gauge data that were gridded to the 0.125° resolution using the synergraphic mapping algorithm
226 with topographic adjustment to the monthly precipitation climatology (Maurer et al., 2004). They
227 reported that the modeled precipitation out of the 4-km resolution was much improved over that
228 out of the coarser 36- or 12-km resolutions.

229 The time series of daily mean wind speed, air temperature, and RH, as well as daily total
230 precipitation averaged over the monitoring sites is illustrated in Figure 1s in the supplement
231 material. It echoed the above findings based on the Taylor diagram. It appeared that NU-WRF
232 constantly overestimated surface wind speed throughout the year with large overestimate occurring
233 in fall and winter, while it severely underestimated RH in summer. Uncertainty in representation
234 of land surface characteristics at least partially explained these biases (Yu, 2014; Gao et al., 2018).
235 High-resolution grid tended to reduce the uncertainty in land surface representation, which would
236 be helpful to improving model performance in meteorology simulation. A more detailed
237 exploration of model-observation mismatch was insightful but beyond the scope of this research.
238

239 3.1.2. Air quality

240 The difference seen in the aforementioned meteorology would cause varied performances
241 on air quality simulations at various model horizontal resolutions. In this study, the NU-WRF
242 simulated surface air quality was compared to the corresponding observations. The 2010 ground-
243 level air quality data were obtained from the Chinese Ecosystem Research Network (CERN,
244 <http://www.cern.ac.cn>) operated by the Institute of Atmospheric Physics of Chinese Academy of
245 Sciences. There were 25 monitoring sites distributed within a 500 km by 500 km area centering
246 around Beijing, China (open diamond in Figure 1). The site locations and characteristics were
247 listed in Table 1. 22 out of 25 sites were either in an urban or a suburban setting, with the balance
248 being in a rural setting. Each site reported hourly concentrations of at least one of the following
249 six pollutants – ozone (O₃), nitrogen oxides (NO_x), carbon monoxide (CO), sulfur dioxide (SO₂),
250 and particulate matters with aerodynamic diameters less than 2.5 and 10 μm (PM_{2.5} and PM₁₀).
251

252 a. Regional average

253 First, the regional mean (averaged across 25 sites) daily surface concentrations from both
254 observations and simulations, paired in space and time, were calculated. The *r*, *NME*, and *NSD*
255 were then computed and illustrated in a Taylor diagram (Figure 2 (bottom row)).

Deleted: best

257 The six pollutants can be put into two groups – one most relevant to ozone photochemistry
258 including O₃, NO_x, and CO, and the other closely tied to aerosols including SO₂, PM_{2.5}, and
259 PM₁₀. It was readily seen that the *r* values of O₃, NO_x, and CO were not very sensitive to the
260 choice of model horizontal resolutions. For O₃, the *r* values for 45-km, 15-km, and 5-km grids
261 were all around 0.85. The respective *r* values were 0.84, 0.81, 0.80 for NO_x, and 0.80, 0.75, 0.73
262 for CO. In general, however, NU-WRF reproduced the observed variations in O₃, NO_x, and CO
263 better with a fine resolution than with a coarse one. *NSD* of 1.23 for O₃ at 5-km resolution was the
264 closest to 1 among three resolutions (1.24 for 15-km and 2.01 for 45-km). *NSDs* were 0.40, 0.36,
265 0.46 for NO_x, and 0.24, 0.27, 0.31 for CO, under the 45-km, 15-km, and 5-km resolutions,
266 respectively, suggesting that simulations with the finest resolution tended to reproduce the
267 observed variations better than the ones with coarse resolutions for these three trace gases.
268 Meanwhile, NU-WRF yielded the smallest bias when employing the fine resolution grid. *NMBs*
269 for O₃ decreased from 115% to 92% when grid resolutions increased from 45-km to 5-km. *NMBs*
270 were -38%, -30%, -18% for NO_x, and -61%, -55%, -51% for CO, under the 45-km, 15-km, and 5-
271 km resolutions, respectively. It was apparent that NU-WRF overestimated surface O₃ but
272 underestimated NO_x and CO, consistent with the findings in the companion MICS-Asia III studies
273 that based their results on ensemble model simulations (Li et al., 2019; Kong et al., 2019). The
274 majority of the air quality monitoring sites used in this study were in an urban setting, which
275 typically were in a VOC-limited regime. This meant that the underestimate of NO_x would reduce
276 the titration that consumed surface O₃ leading to its overestimate. We further analyzed the model
277 bias for daytime (8-18 local standard time) vs. nighttime. It was found that the nighttime biases for
278 surface O₃ and NO_x were approximately 2~4 times higher than those of daytime, consistent with
279 the finding that insufficient NO_x titration caused overestimate of modeled surface O₃.

280 NU-WRF simulated less variations in 3 aerosol related pollutants than those of
281 observations under all applied horizontal resolutions. The *NSDs* ranged from 0.56 (for SO₂ at 15-
282 km resolution) to 0.96 (for PM_{2.5} at 45-km resolution). Though it reproduced the observed SO₂
283 variations the best (*NSD* = 0.68) with 5-km resolution, NU-WRF yielded the best *NSD* for PM_{2.5}
284 (0.96) and PM₁₀ (0.92) when 45-km resolution was employed. Similar to 3 trace gases relevant to
285 surface O₃ formation, the choice of model resolution had a limited effect on *r* statistics. The *r*
286 values varied from 0.70 (45-km resolution) to 0.76 (both 15- and 5-km) for surface SO₂, and from
287 0.68 (45-km resolution) to 0.63 (5-km) for PM_{2.5}. The *r* values for PM₁₀ were all around 0.58
288 under the selected resolutions. The impact of model resolution on *NMBs* showed mixed
289 information – while the smallest *NMBs* for SO₂ (20%) and PM₁₀ (-19%) were achieved using the
290 45-km resolution, the smallest *NMB* for PM_{2.5} (1.5%) was observed at the 15-km resolution. The
291 model underestimate of PM₁₀ was consistent with the findings of the companion investigation
292 using the multi-model ensemble analysis (Chen et al., 2019).

293 Figure 2s in the supplement material shows the time series of daily mean air quality
294 averaged over the monitoring sites for the year 2010. The constant underestimate of CO throughout
295 the year, severe underestimate of NO_x in fall and winter, and large underestimate of SO₂ in summer
296 all pointed out that the emissions inventory may be incomplete, agreeing with the reports by Kong
297 et al. (2019) and Li et al. (2019). In the future, improvement of the emissions inventory accuracy
298 and more realistic temporal emissions distribution may help improving NU-WRF performance in
299 simulating O₃ photochemistry.

300

301

302

b. Individual site

Moved down [1]: In the future, improvement of the emissions inventory accuracy and more realistic temporal emissions distribution may help improving NU-WRF performance in simulating O₃ photochemistry.

Formatted: Subscript

Moved (insertion) [1]

307 The daily average concentrations of each pollutants were calculated and paired in space
308 and time at each air quality monitoring site. Then the statistics at each individual site was computed.

309 Figure 3 illustrates the comparisons of *MB*, *RMSE*, and correlation coefficient (*r*) of surface
310 O₃ from different horizontal resolutions at each site. It can be found that there was no single
311 resolution that yielded the best correlation across all sites. For example, the simulation with the
312 45-km horizontal resolution gave the best correlation over sites BD, CFD, CZ, HJ, SJZ, SQL, TG,
313 TJ, TS, XH, XL, YF, YJ, and ZJK. On the other end of spectrum, BJT, DT, and LTH achieved the
314 best correlation when the 5-km grid was applied. QHD saw the best correlation out of the
315 simulation with the 15-km resolution. In any cases, however, the variations of *r* values from
316 different horizontal resolutions at each site were small (less than 0.04). On the other hand, NU-
317 WRF yielded the worst *MB* and *RMSE* when employing the 45-km resolution grid, while *MB* and
318 *RMSE* were similar between simulations with 15-km and 5-km resolutions. Typically, at sites with
319 urban/suburban settings, *MB* (*RMSE*) based on the 45-km grid was approximately 15~30%
320 (20~40%) higher than that out of the 15-km or 5-km grids. It appeared that NU-WRF tended to
321 have a better performance on ground-level O₃ simulation when increasing the horizontal resolution
322 from 45-km to 15-km, but further finer resolution had diminished impact on improving surface O₃
323 modeling. This was consistent with the finding by Valari and Menut (2008) who concluded that
324 the benefit of finer horizontal resolution grid to improving surface O₃ forecast skill would diminish
325 at certain point.

326 Figure 4 shows the PM_{2.5} case of comparisons of *MB*, *RMSE*, and *r*. Only 10 sites reported
327 PM_{2.5} measurements over year 2010. In general, the NU-WRF simulation with the 45-km grid
328 correlated better to the respective observations than the other 2 resolutions. The only exception
329 was site BD that saw the best correlation for the 5-km resolution. *MB* and *RMSE* results were
330 mixed with no single resolution giving superior results across all sites. Over 2 rural sites (LS and
331 XL), the simulations with the 15-km or 5-km grids yielded remarkably smaller *MB* but correlated
332 less to the corresponding observations than the one with the 45-km grid. Over 8 urban/suburban
333 sites, BD, SQL, and TG experienced the smallest *MB* when employing the 5-km resolution grid,
334 while TG, TJ, and XH saw the least bias at the 45-km resolution. The smallest *MB* at BJT and
335 LTH occurred using the 15-km grid.

336 At the individual site level, the impact of grid resolution on surface NO_x and CO (figures
337 not shown) modeling was similar to that at the regional average. Finer resolution simulation
338 generally reduced *MB* and *RMSE*. The results out of the 45-km grid always had the largest bias.
339 The underestimates of NO_x at least partially explained the overestimate of surface O₃ at each site
340 due to a less efficient NO-titration of O₃. This suggested that a higher resolution modeling with
341 more accurate spatial representation of NO_x emissions would help improving its performance on
342 surface O₃ simulations.

343 The signals for SO₂ and PM₁₀ (figures not shown) simulations were mixed as well. For
344 example, the largest bias for SO₂ simulation over sites BD, CZ, GA, HS, LS, QA, QHD, XH, XL,
345 YF, and YJ occurred when applying the 45-km grid, while the maximum bias over BJT, DT, HJ,
346 LF, LTH, SJZ, SQL, TG, TJ, TS, ZJK, and ZZ happened at the 5-km resolution. Sites CD and
347 CFD saw the largest bias at the 15-km resolution. Unlike PM₁₀ that was almost always
348 underestimated at each site regardless of grid resolutions, SO₂ was overestimated at 18 out of 25
349 sites and underestimated at the remaining 7 sites.

350 An effort has been put to identify the potential reasons that caused the model-observation
351 discrepancy. First and as discussed previously, the spatial distribution of emissions was one key
352 to determining air quality forecast accuracy. Figure 3s shows the typical time evolutions of surface

353 O₃ and NO_x over the rural (XL) and urban (QHD) sites. It can readily be seen that NO_x was
354 underestimated at the urban site but overestimated at the rural site. The coarser the grid resolution,
355 the severer the underestimates/overestimates were. This indicated that the 45-km resolution tended
356 to smooth out emissions to make urban (or emissions centers) less polluted but rural more polluted.
357 It in turn led to an overestimate of surface O₃ over the urban sites mainly due to the reduced NO_x
358 titration effect, especially at night when there was no photochemical O₃ formation. The statistics
359 showed that the bias of the modeled daytime (7 am ~ 7 pm local time) average surface O₃ was 30%
360 ~ 90% smaller than that of the daily average in the urban sites, no matter which grid resolution
361 was applied. This suggested that in the future the high-resolution emissions, especially proper
362 representation of emission gradients, would be helpful in improving air quality prediction. The
363 effect of emissions gradients associated with the grid resolution would be further discussed in the
364 inter-model comparison section.

365 Next, the driving meteorology, especially wind, was important to accurately forecast air
366 quality over coastal areas that bore sharp thermal contrasts. QHD site locates approximately 5 km
367 from the ocean and is subject to sea breeze effects. The detailed analysis of meteorology and air
368 quality over QHD was conducted. The results indicated that the choice of grid resolution had large
369 impacts on model simulations at this coastal site. The selection of the 5-km grid reduced biases of
370 both surface temperature and wind speed. The biases of temperature reduced from 1.22 K (45-km)
371 to -0.42 K (15-km), and further down to -0.31 K when the 5-km grid was applied. The biases of
372 surface wind speed for the 45-km, 15-km, and 5-km grids were 3.72, 4.19, and 1.95 m s⁻¹,
373 respectively. The improvement of meteorology forecast helped reducing the biases of air quality
374 modeling. The biases of O₃/NO_x for the 45-km, 15-km, and 5-km resolution grids were 29.94/-
375 22.46 ppbv, 24.09/-20.29 ppbv, 23.97/-17.95 ppbv, respectively. The improvement using the 15-
376 km grid over the 45-km grid was remarkable but that using the 5-km grid over the 15-km grid was
377 marginal. The result emphasized the importance of high-resolution modeling to improvements of
378 air quality forecast skills, especially at coastal and complex terrain areas (e.g., QHD and XL).

379
380
381 **c. Extreme values**

382 High concentrations of air pollutants are of more concerns because of their adverse health
383 effects on both human beings and ecosystem. High pollutant concentrations also pose a greater
384 risk for non-compliance of the ambient air quality standards. Therefore, evaluations of impacts of
385 grid resolution on extreme concentrations of air pollutants are desirable.

386 Figure 5 displays the probability density function distributions of six pollutants based on
387 hourly surface concentrations across the monitoring sites. This analysis was focused on high
388 pollutant concentrations with the cutoff values for CO, O₃, NO_x, SO₂, PM_{2.5}, and PM₁₀ being
389 1.1 ppmv, 60 ppbv, 25 ppbv, 5.5 ppbv, 15 µg m⁻³, and 30 µg m⁻³, respectively. It appeared that
390 NU-WRF, regardless of the grid resolutions, failed to simulate surface CO with concentrations
391 more than 4 ppmv, likely due to the underestimate of CO emissions (Kong et al., 2019). The grid
392 resolution appeared to have limited impacts on surface PM₁₀ simulations when its concentrations
393 were more than 200 µg m⁻³. On the other hand, the grid resolution showed large impacts on NU-
394 WRF's capability in simulating high surface concentrations of O₃, NO_x, SO₂, and PM_{2.5}. For
395 surface O₃ with concentrations more than 100 ppbv, the NU-WRF results with the 45-km grid
396 appeared to better agree with the probability distribution of observations. For surface NO_x with
397 concentrations more than 70 ppbv, the NU-WRF results with the 5-km resolution grid better
398 mimicked the observed distribution. Modeling with the 5-km grid also yielded the best results of

Formatted: Subscript
Formatted: Font: (Default) Times New Roman, 12 pt

Formatted: Font: (Default) Times New Roman, 12 pt
Formatted: Subscript
Formatted: Font: (Default) Times New Roman, 12 pt
Formatted: Font: (Default) Times New Roman, 12 pt
Formatted: Font: (Default) Times New Roman, 12 pt
Formatted: Font: (Default) Times New Roman, 12 pt
Formatted: Font: (Default) Times New Roman, 12 pt
Formatted: Font: (Default) Times New Roman, 12 pt
Formatted: Justified
Formatted: Font: (Default) Times New Roman, 12 pt
Formatted: Font: (Default) Times New Roman, 12 pt
Formatted: Font: (Default) Times New Roman, 12 pt

Formatted: Subscript
Formatted: Font: (Default) Times New Roman, 12 pt

Formatted: Font: (Default) Times New Roman, 12 pt

399 distributions, in comparisons to the respective observations, of SO₂ with concentrations more than
400 45 ppbv, and of PM_{2.5} with concentrations greater than 120 µg m⁻³.

401 Table 2 lists the occurrences of violations of China's national ambient air quality standards
402 (NAAQS) for the six pollutants from both observations and simulations, in which columns "Class
403 1" and "Class 2" list the standards for rural and urban-suburban sites, respectively, and column
404 "Frequency" indicates the time integration of each NAAQS. It was apparent that NU-WRF failed
405 to report CO violations at any grid resolutions. No CO NAAQS violation was simulated but the
406 observation showed that surface CO exceeded the national standard by more than 1000 times. NU-
407 WRF underestimated the NAAQS exceedances of NO_x and SO₂. A higher-resolution grid
408 appeared to be able to catch more violations although the modeled results at the 5-km resolution
409 only captured 33% and 10% observed exceedances of NO_x and SO₂, respectively. NU-WRF
410 overestimated surface O₃ and PM_{2.5} when their concentrations were more than the corresponding
411 NAAQS. The fine grid resolution (i.e., 5-km) appeared to reduce the overestimation of surface O₃
412 exceedances largely as compared to the 45-km grid but only marginally compared with the 15-km
413 grid. Compared to the observed occurrences of surface O₃ standard violation (3,684), the simulated
414 exceedances were 6.7, 2.8, and 2.7 times higher when employing the 45-km, 15-km, and 5-km
415 resolution grid, respectively. The observations showed 1,343 occurrences of surface PM_{2.5}
416 exceedances, while the modeled exceedances were 377, 267, and 231 more for the 45-km, 15-km,
417 and 5-km grids, respectively. As for surface PM₁₀, the modeled exceedances were approximately
418 27%, 43%, and 41% less than the observed one for the 45-km, 15-km, and 5-km grids, respectively.
419

420 3.2. Inter-resolution comparisons

421 It is informative to compare the NU-WRF results out of different horizontal resolutions.
422 This, in addition to the discussion in section 3.1.2.b, can help understand the reasons why model
423 resolution matters.
424

425 3.2.1. Emissions

426 There were two types of emissions applied in this study. One was the prescribed emissions
427 out of the anthropogenic and wild fire sources, and the other was emissions computed online using
428 the real-time meteorology (or dynamic emissions) including emissions from biogenic sources, dust
429 sources, and sea spray. Amounts and temporal variations of dynamic emissions depended on
430 surrounding environmental conditions. For example, air temperature and solar radiation regulates
431 biogenic emissions (Guenther et al., 2006). Surface wind speed plays a major role in both dust
432 (Ginoux et al., 2001; Chin et al., 2002) and sea salt emissions (Gong, 2003).

433 For the prescribed emissions, the differences of domain total masses out of each grid were
434 small (less than 5%). However, the emission gradient around sources of a fine resolution grid
435 appeared to be sharper than that of a coarse resolution grid. This meant that a coarse grid tended
436 to distribute the prescribed emissions more evenly into the domain, while a fine grid tended to
437 produce more extreme concentrations of primary pollutants (emitted directly from a source) such
438 as NO_x and SO₂, as shown in Table 2.

439 Online calculated emissions, on the other hand, displayed large differences in both gradient
440 and total mass. Similar to the case of prescribed emissions, a fine resolution grid tended to give a
441 sharper gradient of dynamic emissions than a coarse resolution grid did, as highlighted in Figure
442 6 (1st row) that illustrated the biogenic isoprene emissions (mol km⁻² hr⁻¹) on a typical summer day.
443 It was apparent that much more details were simulated using a fine resolution grid - the flow of
444 Yellow River can even be seen on the 5-km resolution map that was otherwise invisible from the

Deleted: .

446 coarser resolution maps. Meanwhile, the total masses of dynamic emissions showed large
447 difference out of different resolution grids as listed in Table 3. On an annual basis, the domain
448 total isoprene emissions were 740,562 tons when estimated using the 45-km grid, approximately
449 85% and 86% of those with the 15-km and 5-km grids, respectively. The total dust emissions out
450 of the 45-km grid were 2,431 tons, only 54% and 62% of those based on the respective 15-km and
451 5-km grids. The percentage contrasts for sea salt emissions were even larger with emissions out of
452 the 15-km and 5-km grids being 1.3 and 1.6 times more than those of the 45-km grid, respectively.
453 It should be noted that although they differed greatly between out of the 45-km and 15-km grids,
454 the dynamic emissions out of the 5-km grid were much closer to those out of the 15-km grid,
455 partially explaining why the impact of model resolution on surface air quality was less remarkable
456 by increasing the resolution from 15-km to 5-km than from 45-km to 15-km.

457 The spatial (gradient) and mass variations in emissions out of different resolution grids
458 would result in difference in air quality simulations.

459 3.2.2. Meteorology

460 It's been reported that simulated meteorology varies in response to selections of model grid
461 resolutions (e.g., Tie et al., 2010; Lee et al., 2018). Meteorology plays an important role in
462 regulating regional air quality – it affects emissions amount originating from biogenic, dust, and
463 sea sources; it impacts atmospheric chemical and photochemical transformation; and it directs air
464 flows and the associated transport of trace gases and aerosols. In this investigation, a few
465 meteorological parameters key to air pollutant generation and accumulation were analyzed,
466 including surface wind, air temperature, downward shortwave flux at surface (SWDOWN),
467 planetary boundary layer height (PBLH), and cloud water (liquid + ice) path (CWP). We focused
468 on months that were prone to deteriorated PM_{2.5} (January) and O₃ (July) air quality as shown in
469 Figure 6 and Table 3.

470 NU-WRF simulated a similar direction of surface wind in July 2010 over the eastern
471 portion of the domain (2nd row of Figure 6). In general, average wind speed was larger over Bohai
472 Sea and Yellow Sea than over the surrounding land areas with dominating wind direction being
473 south and southeast. Based on the results from the 15-km and 5-km grids, the peak average wind
474 speeds over 4 m s⁻¹ were found in Bohai Bay blowing to Tianjin and Beijing. However, such a
475 peak was absent from the 45-km grid simulation. In the west portion of the domain, the wind
476 direction changed from southeast in the south to southwest in the north in general. Compared to
477 the more organized wind directions out of the 45-km grid, wind directions out of the 15- and 5-km
478 grids were more chaotic. Averaged over the domain, the January mean wind speed out of the 45-
479 km grid was 2.92 m s⁻¹, which were 7% and 16% larger than those of the 15-km and 5-km grids,
480 respectively. The largest July mean wind speed was again simulated with the 45-km grid, 10% and
481 12% larger than the corresponding wind speed out of the 15-km and 5-km grids, respectively.

482 Overall, NU-WRF simulated very similar magnitudes and spatial patterns of surface air
483 temperature in July (3rd row of Figure 6), regardless of the selections of grid resolutions. Large
484 portions of the NCP experienced more than 300 K of July average air temperature. The minimum
485 average temperature of approximately 290 K was found in the central north part of the domain,
486 which was part of the Mongolian Plateau with the elevation being over 1,500 m above the sea level.
487 The domain average January and July surface air temperature were around 268 K and 300 K,
488 respectively, for simulations out of all three grids.

489 As expected, the modeling results from all three grids (4th row of Figure 6) showed that
490 July average PBLH over sea was much smaller than that over land. The ~~large~~ average PBLH (more
491

Deleted: maximum

493 than 1,000 m) was found in the northwestern corner of the domain with a dominant land cover
494 type of grassland mosaiced with open shrubland that appeared to be drier than the other land cover
495 types in the domain. The high sensible heating associated with dry soil tended to produce the deep
496 PBL (Tao et al., 2013). The largest domain-average PBLHs in January and July were found from
497 the simulations out of the 15-km and 45-km grids, respectively. In January, the differences of the
498 domain-average PBLHs from different grid resolutions were small and within 2%. In July,
499 however, such difference can be over 9%.

500 Regardless of the grid resolutions, NU-WRF simulated a generally southeast-northwest
501 gradient of SWDOWN in July with the highest flux (over 300 W m⁻²) occurring in the northwestern
502 domain (5th row of Figure 6). The differences between the maximum and minimum domain
503 average SWDOWN out of 3 grids were 5.6% and 3.3% in January and July, respectively.

504 CWP represented the vertical integration of cloud water (including both liquid and ice
505 phases) contents and can be regarded as a proxy of cloud amount and coverage. Opposite to the
506 SWDOWN case, NU-WRF modeled a generally northwest-southeast gradient of CWP in July with
507 the high values found in the southeastern domain (6th row of Figure 6). This was understandable
508 since cloud reflects and scatters the incoming solar radiation and thus affect SWDOWN. Large
509 cloud existence tended to reduce the solar flux reaching the underneath Earth surface. The CWP
510 differences among the model results out of different grid resolutions appeared to be larger than
511 SWDOWN differences. In July, the domain average CWPs out of the 15-km and 5-km grids were
512 37% and 33% larger than that of the 45-km grid, respectively. The gaps were even larger in January,
513 during which the domain average CWPs from the 15-km and 5-km grids were approximately 1.6
514 times larger than that from the 45-km grid.

515 3.2.3. Air Quality

516 In response to the aforementioned emissions and meteorological variations resulted from
517 the selections of model grid resolutions, changes in regional air quality ensued as illustrated in
518 Figure 7 and Table 3. This figure shows the July average concentrations of ground-level O₃ and
519 its precursors of NOx and CO, as well as the January mean concentrations of surface SO₂, PM2.5,
520 and PM10, during which month the respective pollutants tended to reach high concentrations.

521 O₃ is a secondary pollutant that is formed in the atmosphere through complex
522 photochemical processes upon existences of its precursors such as NOx and volatile organic
523 compounds (VOC). Figure 7 (row 1) shows that the spatial distributions of surface O₃ are similar
524 to each other but the concentrations out of the 15-km and 5-km grids are smaller than those from
525 the 45-km grid. The domain average surface O₃ concentration in July was approximately 87 ppbv
526 based on the results from the 45-km grid, 26% and 25% higher than those out of the 15-km and 5-
527 km grid, respectively. In January, however, the highest domain average concentration occurred
528 when the 5-km grid was used, which was 5.3% higher than that out of the 45-km grid.

529 For the primary pollutants, i.e., NOx, CO, and SO₂ (rows 2-4 of Figure 7, respectively),
530 which were emitted directly by their sources, the spatial distributions of their concentrations
531 mimicked closely with their emission distributions. High concentrations centered around emission
532 sources with a reducing gradient outward. The domain average concentrations of these 3 pollutants
533 out of the 45-km grid results were always the largest in both January and July. The average surface
534 NOx concentrations from the simulations out of the 15-km and 5-km grids were around 24% lower
535 than their counterparts out of the 45-km grid in January. In July, the differences were reduced to
536 7.9% and 11.8% for the 15-km and 5-km grids, respectively. On the other hand, the larger
537 percentage differences, as compared to the results out of the 45-km grid, occurred in July than in

Deleted: portion

Deleted: , also in the Mongolian Plateau

541 January for both CO and SO₂. For example, the surface CO concentrations out of the 5-km grid
542 were 12.3% and 30.6% lower than those based on the 45-km grid in January and July, respectively.
543 The respective ground-level SO₂ concentrations from the 5-km grid were 20.5% and 38.9% lower
544 than those from the 45-km grid in January and July.

545 It was interesting to note that among the 3 cases, the domain average July surface O₃ and
546 NO_x concentrations were both the highest out of the 45-km grid, contrary to the results discussed
547 in section 3.1.2a where the highest O₃ concentration occurred out of the simulation using the 45-
548 km grid while the highest NO_x concentration happened with the 5-km grid. This seemingly
549 contradicting result was internally consistent. Section 3.1.2a actually depicted the average surface
550 concentrations in an urban environment (23 of 25 monitoring sites were in an urban/suburban
551 setting), where surface O₃ formation was typically VOC controlled such that NO tended to
552 consume O₃ through titrations. As discussed in section 3.2.1, a 5-km grid gave a much sharper
553 emissions gradient with anthropogenic emissions concentrating in urban/suburban areas. This led
554 to higher NO_x concentrations around urban/suburban areas out of the simulation with the 5-km
555 grid, which effectively resulted in lower O₃ concentrations there through the NO titration effect.
556 The domain average discussed in this section, however, was the average covering the vast rural
557 area that generally was NO_x-limited such that surface O₃ formation was controlled by the
558 availability of NO_x – more NO_x resulting in more O₃ through photochemical processes. In this
559 case, the 45-km grid tended to distribute NO_x emissions more evenly in the region, effectively
560 decreasing the surface NO_x concentration in urban areas but increasing it over rural areas. The
561 larger average July wind speed simulated by the 45-km grid (Figure 6 and Table 3) further
562 smoothed out the NO_x distribution in NCP. This in turn increased the domain average surface O₃
563 concentration via photochemistry based on the 45-km resolution results. In addition, vertical lifting
564 played an important role in explaining the maximum regional O₃ in July simulated by the 45-km
565 grid as compared to the results by the other two grid resolutions. As displayed in Figure 4s in the
566 supplemental material, a fine resolution modeling (e.g., 5-km) tended to produce a stronger updraft
567 than a coarse resolution modeling (e.g., 45-km), consistent with the findings by Lee et al. (2018).
568 The strong uplift would bring more surface pollutants such as NO_x into the upper atmosphere, thus
569 further reducing the NO_x availability at ground limiting the surface ozone production but
570 increasing its formation in the upper atmosphere.

571 Vertical distributions of O₃ also tend to have a sizable impact on next day's surface O₃
572 levels (e.g., Kuang et al., 2011; Caputi et al., 2019). Figure 8 illustrates the domain average profiles
573 of vertical wind, NO_x, O₃ (panels a–c), and the average diurnal distribution of surface O₃ (panel
574 d) over July. Here we limited our discussion on the results from the 15- and 5-km grids since 45-
575 km grid artificially allowed more NO_x emissions spreading to rural areas to produce much more
576 O₃ as shown in the previous paragraph. Lee et al. (2018) claimed that a coarse resolution model
577 appeared to lower updraft as compared with a fine resolution modeling. This study agreed with
578 their finding as illustrated in Figure 8 (panel a). The domain average July vertical wind out of the
579 simulation with the 5-km grid ranged from 0.25 to 0.45 cm s⁻¹ (upward) between 800 hPa and 400
580 hPa, stronger than the corresponding one out of the 15-km grid. The reason was complex and the
581 aerosol-cloud interaction induced freezing/evaporation-related invigoration mechanism played a
582 role (Lee et al., 2018). The stronger upward wind tended to lift more gaseous pollutants up to the
583 free troposphere as shown in Figure 8 (panel b (NO_x) and c (O₃)). The pollutants there would have
584 visible impacts on the following-day surface air quality, especially on O₃ levels at night and in the
585 morning when sun breaks out the nocturnal planetary boundary layer, as evidenced in Figure 8
586 (panel d). At night with no photochemical formation, surface O₃ concentration was largely

Formatted: Subscript

Formatted: Font: (Default) Times New Roman, 12 pt

Formatted: Font: (Default) Times New Roman, 12 pt

Formatted: Font: (Default) Times New Roman, 12 pt

Deleted: In addition, the higher air temperature and stronger SWDOWN in July out of the 45-km grid as compared to other two resolutions favored more surface O₃ generations.

590 controlled by upper-level O₃ mixing down, NO titration and O₃ dry deposition. With the virtually
591 same average surface NO concentrations out of the 15- and 5-km grids, the upper-level O₃ mixing
592 down appeared to control the relative magnitudes of surface O₃ concentrations simulated using the
593 15- and 5-km grids. This partially explained why, at night and early morning, the ground level O₃
594 concentrations were higher out of the 5-km grid than from the 15-km grid. During daytime when
595 the photochemical formation of O₃ takes control, the regional average surface O₃ concentrations
596 is largely determined by the availability of O₃ precursors (i.e., NO_x and VOC) and ambient
597 environmental conditions. In this case, more spreading NO_x emissions out of the 15-km grid
598 appeared to generate more surface O₃ than the 5-km grid did.

599 PM_{2.5} and PM₁₀ were mixed pollutants that not only were emitted by various sources but
600 also were generated in the atmosphere through physical and chemical processes. Figure 7 shows
601 that high surface concentrations of PM_{2.5} (more than 120 μg m⁻³, row 5) and of PM₁₀ (more than
602 170 μg m⁻³, row 6) were still found around the source areas based on the modeling results out of
603 the 15-km and 5-km grids. However, high PM_{2.5} and PM₁₀ concentrations spread out to larger
604 areas based on the results from the 45-km grid as compared to the ones from the finer grid
605 resolutions. Similar to the primary pollutants, the largest domain average surface concentrations
606 occurred when a 45-km grid was used for the NU-WRF simulation. The domain average PM_{2.5}
607 concentrations out of the 15-km and 5-km grids in January were 15.7% and 14% lower than those
608 from the 45-km grid, respectively. The surface PM_{2.5} concentration differences among results out
609 of different grid resolutions grew larger in July, reaching 48% when comparing the result from the
610 5-km grid to that from the 45-km grid. The domain average surface PM₁₀ concentrations showed
611 similar pattern to that of PM_{2.5} with the results out of the 5-km grid being 12.2% and 44.2%
612 smaller than that from the 45-km grid.

613 It is worth noting that the magnitudes and spatial distributions of ground-level pollutants
614 were close to each other between the results out of the 15-km and 5-km grids. This again indicates
615 that the improvement of fine grid resolution modeling reduces at a certain point. In future MICS-
616 Asia efforts, a 15-km grid appears to offer the optimized results balanced with performance and
617 resources.

618 619 **4. Summary**

620 Contributing to MICS-Asia Phase III whose goals included identifying and reducing air
621 quality modeling uncertainty over the region, this investigation examined the impact of model grid
622 resolutions on the performances of meteorology and air quality simulation. To achieve this, NU-
623 WRF was employed to simulate 2010 air quality over the NCP region with three grid resolutions
624 of 45-km, 15-km, and 5-km. The modeling results were compared to the observations of surface
625 meteorology archived by CMA, and of ground-level air quality collected in CERN. The inter-
626 model comparison among the simulation results out of three grids were also conducted to
627 understand the reasons why model resolution mattered.

628 The analysis showed that there was no single resolution which would yield the best
629 reproduction of meteorology and air quality across all monitoring sites. From a regional average
630 prospective (i.e., across all monitoring sites in this study), the choice of grid resolution appeared
631 to have a minimum influence on air temperature modeling but affected wind, RH, and precipitation
632 simulation profoundly. A 5-km grid appeared to give the best wind simulation as compared to the
633 observations quantified by bias, RMSE, standard deviation, and correlation. Compared to the one
634 using the 45-km grid, the simulated wind speed from a 5-km grid reduced the positive bias by
635 46.8%. While a 15-km grid yielded the best overall performance on RH modeling, the result out

636 of the 45-km grid gave the most realistic reproduction of precipitation. The statement on
637 precipitation should be taken with caution since it was based on the comparison with the site
638 observations. Seeing the very heterogeneous nature of precipitation, the penalty of model hitting
639 or missing a rain event was severe. Thus, the coarse grid covering more areas within a grid cell
640 would reduce chances of mistaken precipitation hitting or missing simulations. However, a
641 comparison of modeled precipitations to gridded “observation” that was re-constructed using the
642 synergraphic mapping algorithm with topographic adjustment to the monthly precipitation
643 climatology showed opposite result, where the fine resolution modeling showed superior
644 reproduction of precipitation than the coarse resolution simulation (Gao et al., 2017).

645 The simulated meteorology differences due to the selection of grid resolution would
646 consequently lead to differences in air quality simulation. Air pollutant concentrations were
647 basically determined by their emissions and underlying meteorology that directed their formation
648 (e.g., O₃ and aerosols), transport, and removal processes. For the prescribed emissions originated
649 from anthropogenic and wild fire sources, the grid resolution had limited influence on emission
650 amount – less than 5% difference with each other under the different resolution grids – but large
651 impact on emission spatial distribution with sharper emission gradient around sources out of a fine
652 resolution grid than from a coarse resolution one. For the dynamic emissions driven by
653 meteorology, not only was an emission gradient around a source larger out of a higher resolution
654 grid, but also the total emission amount varied greatly. For example, the domain total annual
655 biogenic isoprene emissions from a 5-km grid was about 16% larger than those out of a 45-km
656 grid due to the underlying differences in land cover and meteorology.

657 Though the impact of grid resolution on air quality varied from location to location, finer
658 grid yielded better results for daily mean surface O₃, NO_x, CO, and PM_{2.5} simulations from a
659 regional average perspective. For example, after reducing the grid resolution from 45-km to 15-
660 km, the positive bias of daily mean surface O₃ and PM_{2.5} decreased by 15% and 75%, respectively.
661 Fine resolution modeling was especially beneficial to high pollutant concentration forecast. This
662 was important to air quality management. Taking China’s NAAQS as cutoff values for each
663 pollutant, the frequencies of noncompliance occurrences of O₃, NO_x, SO₂, and PM_{2.5} out of the
664 5-km grid simulation were much closer to the observations than those out of the 45-km modeling
665 were. For example, the simulation with the 5-km grid produced 168% and 17% more exceedances
666 in NAAQS of O₃ and PM_{2.5}, respectively, whereas the respective exceedances were 573% and
667 28% more with modeling using the 45-km grid, as compared to the observed exceedances. It also
668 was worth noting that the benefit of increasing grid resolution to better surface O₃ and PM_{2.5}
669 simulations started to diminish when the horizontal resolution reached 15-km, agreeing with the
670 finding by Valari and Menut (2008). There was a caveat, though. The anthropogenic MIX and fire
671 GFEDv3 emissions inventories bore the 0.25° by 0.25° and 0.5° by 0.5° resolution, respectively.
672 These resolutions cannot resolve the 5-km grid. Should a 5-km resolution emissions inventory be
673 available and used, the benefit of high-resolution modeling would likely have been more
674 prominent.

675 It should be pointed out that NU-WRF significantly overestimated surface O₃ concentration
676 but underestimated ground-level CO and NO_x concentrations regardless of grid resolutions. This
677 was true not only on the regional averages but also at majority of the monitoring sites. The missing
678 emissions was believed to be largely responsible for this result (Kong et al., 2019). Underestimate
679 of surface NO_x tended to increase ground-level O₃ due to the reduced titration effect, especially at
680 night over urban areas that were typically NO_x abundant.

Deleted: s

Deleted: -

Formatted: Subscript

Deleted:

Deleted: .

685 In conclusion, grid resolution had a profound effect on NU-WRF performance on
686 meteorology and air quality over the East Asia. Fine resolution grid did not always generate the
687 best modeling results and the proper selection of horizontal resolution hinged on investigation
688 topics for a given set of physics and chemistry choices in a model. With regard to MICS-Asia
689 Phase III whose major goal was to examine regional air quality, in general, the finer the grid
690 resolution was, the better the simulation results would be. This was especially true over the coastal
691 areas and complex terrains where a sharp local energy gradient existed. Fine resolution grid was
692 also extremely helpful to reproducing pollutants at higher concentrations that were most relevant
693 to air quality planning and management. However, the benefit of high resolution was not linear
694 with the decrease of grid size. At certain point, the improved modeling accuracy due to an increase
695 in grid resolution was so marginal that it cannot justify the computational cost associated with the
696 fine grid simulation. Based on the balance of modeling accuracy and efficiency, a 15-km horizontal
697 grid appeared to be an appropriate choice to optimize model performance and resource usage if
698 the study domain remained unchanged for future MICS-Asia activities. The study suggested that
699 the high-resolution emissions, especially the proper representation of emission gradients, would
700 be helpful in improving air quality prediction. Moreover, the profile measurements of both
701 meteorology and air quality, in supplement with the ground monitoring networks, would be greatly
702 helpful to identifying model deficiencies and thus improving model forecast skills.

Deleted: .

704 **Competing interests**

705 The authors declare that they have no conflict of interest.

706

707 **Author contribution**

708 ZT and MC designed the experiments. ZT, MG, TK, DK, and HB carried out the
709 experiments working on various modeling components. YW and ZL collected, organized, and
710 archived the ground air quality measurement data. All authors contributed to model result analysis
711 and interpretation. ZT prepared the manuscript with contributions from all co-authors.

712

713 **Acknowledgement**

714 This work was supported by the NASA's Atmospheric Composition: Modeling and
715 Analysis Program (ACMAP) and Modeling, Analysis, and Prediction (MAP) program. The
716 authors thank MICS-Asia for its organized platform of discussion and data sharing. This work is
717 not possible without the supercomputing and mass storage support by NASA Center for Climate
718 Simulation (NCCS). All data collected and generated for this research are archived and stored on
719 NCCS servers. Due to the sheer size of data, it is impractical to upload data to a public domain
720 repository. However, the authors will be happy to share data on an individual request basis.

721

722

724 **References**

- 725 Akimoto, H., Mori, Y., Sasaki, K., Nakanishi, H., Ohizumi, T., and Itano, Y.: Analysis of
726 monitoring data of ground-level ozone in Japan for long-term trend during 1990-2010:
727 Causes of temporal and spatial variation, *Atmos. Environ.*, 102, 302-310, 2015.
- 728 Anenberg, S. C., Horowitz, L. W., Tong, D. Q., and West J. J.: An estimate of the global burden
729 of anthropogenic ozone and fine particulate matter on premature human mortality using
730 atmospheric modeling, *Environ. Health Perspect.*, 118(9), 1189-1195,
731 doi:10.1289/ehp.0901220, 2010.
- 732 Cai, W., Li, K., Liao, H., Wang, H., and Wu, L.: Weather conditions conducive to Beijing severe
733 haze more frequent under climate change, *Nature Climate Change*, 7, 257-263,
734 doi:10.1038/NCLIMAE3249, 2017.
- 735 Caputi, D. J., Faloona, I., Trousdell, J., Smoot, J., Falk, N., and Conley, S.: Residual layer ozone,
736 mixing, and the nocturnal jet in California's San Joaquin Valley, *Atmos. Chem. Phys.*, 19,
737 4721-4740, doi:10.5194/acp-19-4721-2019, 2019.
- 738 Carmichael, G., Calori, G., Hayami, H., Uno, I., Cho, S. Y., Engardt, M., Kim, S. B., Ichikawa,
739 Y., Ikeda, Y., Woo, J. H., Ueda, H., and Amann, M.: The MICS-Asia study: model
740 intercomparison of long-range transport and sulfur deposition in East Asia, *Atmos. Environ.*,
741 36, 175-199, 10.1016/s1352-2310(01)00448-4, 2002.
- 742 Carmichael, G., Sakurai, T., Streets, D., Hozumi, Y., Ueda, H., Park, S., Fung, C., Han, Z., Kajino,
743 M., and Engardt, M.: MICS-Asia II: The model intercomparison study for Asia Phase II:
744 methodology and overview of findings, *Atmos. Environ.*, 42, 3468-3490,
745 10.1016/j.atmosenv.2007.04.007, 2008.
- 746 Chen, L., Gao, Y., Zhang, M., Fu, J. S., Zhu, J., Liao, H., Li, J., Huang, K., Ge, B., Wang, X.,
747 LAM, Y. F., Lin, C.-Y., Itahashi, S., Nagashima, T., Kajino, M., Yamaji, K., Wang, Z., and
748 Kurokawa, J.-I.: MICS-Asia III: Multi-model comparison and evaluation of aerosol over East
749 Asia, *Atmos. Chem. Phys. Discuss.*, <http://doi.org/10.5194/acp-2018-1346>, in review, 2019.
- 750 Chin, M., Ginoux, P., Kinne, S., Torres, O., Holben, B. N., Duncan, B. N., Martin, R. V., Logan,
751 J. A., Higurashi, A., and Nakajima, T.: Tropospheric aerosol optical thickness from the
752 GOCART model and comparisons with satellite and Sun photometer measurements, *J.*
753 *Atmos. Sci.*, 59, 461-483, 2002.
- 754 Chin, M., Diehl, T., Ginoux, P., and Malm, W.: Intercontinental transport of pollution and dust
755 aerosols: implications for regional air quality, *Atmos. Chem. Phys.*, 7, 5501-5517,
756 doi:10.5194/acp-7-5501-2007, 2007.
- 757 Chou, M.-D. and Suarez, M. J.: A solar radiation parameterization (CLIRAD-SW) for atmospheric
758 studies, NASA Tech. Rep. NASA/TM-1999-10460, vol. 15, 38 pp, 1999.
- 759 Ek, M. B., Mitchell, K. E., Lin, Y., Rogers, E., Grunmann, P., Koren, V., Gayno, G., and Tarpley,
760 J. D.: Implementation of Noah land surface model advances in the National Centers for
761 Environmental Prediction operational mesoscale Eta Model, *J. Geophys. Res.*, 108, 8851,
762 doi:10.1029/2002JD003296, 2003.
- 763 Emmons, L. K., Walters, S., Hess, P. G., Lamarque, J.-F., Pfister, G. G., Fillmore, D., Granier, C.,
764 Guenther, A., Kinnison, D., Laepple, T., Orlando, J., Tie, X., Tyndall, G., Wiedinmyer, C.,
765 Baughcum, S. L., and Kloster, S.: Description and evaluation of the Model for Ozone and
766 Related chemical Tracers, version 4 (MOZART-4), *Geosci. Model Dev.*, 3, 43-67, 2010.
- 767 Gao, M., Carmichael, G. R., Wang, Y., Saide, P. E., Yu, M., Xin, J., Liu, Z., and Wang, Z.:
768 Modeling study of the 2010 regional haze event in the North China Plain, *Atmos. Chem.*
769 *Phys.*, 16, 1673-1691, doi:10.5194/acp-16-1673-2016, 2016.

770 Gao, M., Han, Z., Liu, Z., Li, M., Xin, J., Tao, Z., et al.: Air quality and climate change, Topic 3
771 of the Model Inter-Comparison study for Asia Phase III (MICS-Asia III) – Part 1: Overview
772 and model evaluation, *Atmos. Chem. Phys.*, 18 (7), 4859-4884, doi:10.5194/acp-18-4859-
773 2018, 2018.

774 Gao, Y., Leung, L. R., Zhao, C., and Hagos, S.: Sensitivity of U.S. summer precipitation to model
775 resolution and convective parameterizations across gray zone resolution, *J. Geophys. Res.*
776 *Atmos.*, 122, 2,714-2,733, doi:10.1002/2016JD025896, 2017.

777 Ginoux, P., Chin, M., Tegen, I., Prospero, J., Holben, B., Dubovik, O., and Lin, S.-J.: Sources and
778 global distributions of dust aerosols simulated with the GOCART model, *J. Geophys. Res.*,
779 106, 20,255-20,273, 2001.

780 Gong, S. L.: A parameterization of sea-salt aerosol source function for sub- and super-micron
781 particles, *Glob. Biogeochemical Cycles*, 17, No. 4, 1097, doi: 10.1029/2003GB002079, 2003.

782 Grell, G. A. and Devenyi, D.: A generalized approach to parameterizing convection combining
783 ensemble and data assimilation techniques, *Geophys. Res. Lett.*, 29, 1693,
784 doi:10.1029/2002GL015311, 2002.

785 Grell, G. A., Peckham, S. E., Schmitz, R., McKeen, S. A., Frost, G., Skamarock W. C., and Eder,
786 B.: Fully coupled “online” chemistry within the WRF model, *Atmos. Environ.*, 39, 6957–
787 6975, 2005.

788 Gross, A. and Stockwell, W. R.: Comparison of the EMEP, RADM2 and RACM Mechanisms, *J.*
789 *Atmos. Chem.*, 44, 151-170, 2003.

790 Guenther, A., Karl, T., Harley, P., Wiedinmyer, C., Palmer, P. I., and Geron, C.: Estimates of global
791 terrestrial isoprene emissions using MEGAN (Model of Emissions of Gases and Aerosols from
792 Nature), *Atmos. Chem. Phys.*, 6, 3181-3210, 2006.

793 Hong, S. Y., Noh, Y., and Dudhia, J.: A new vertical diffusion package with an explicit treatment
794 of entrainment processes, *Mon. Wea. Rev.*, 134, 2318-2341, 2006.

795 Huang, R.-J., Zhang, Y., Bozzetti, C., Ho, K.-F., Cao, J.-J., Han, Y., Daellenbach, K. R., Slowik,
796 J. G., Platt, S. M., Canonaco, F., Zotter, P., Wolf, R., Pieber, S. M., Bruns, E. A., Crippa, M.,
797 Ciarelli, G., Piazzalunga, A., Schwikowski, M., Abbaszade, G., Schnelle-Kreis, J.,
798 Zimmermann, R., An, Z., Szidat, S., Baltensperger, U., Haddad, I. E., and Prevot, A. S. H.:
799 High secondary aerosol contribution to particulate pollution during haze events in China,
800 *Nature*, 514, 218-222, doi:10.1038/nature13774, 2014.

801 Jin, Y., Andersson, H., and Zhang, S.: Air pollution control policies in China: A retrospective and
802 prospects, *Int. J. Environ. Res. Public Health*, 13(12), 1219, doi:10.3390/ijerph13121219,
803 2016.

804 Kim, D., Chin, M., Kemp, E. M., Tao, Z., Peters-Lidard, C. D., and Ginoux, P.: Development of
805 high-resolution dynamic dust source function – A case study with a strong dust storm in a
806 regional model, *Atmos. Environ.*, 159, 11-25, doi:10.1016/j.atmosenv.2017.03.045, 2017.

807 Kong, L., Tang, X., Zhu, J., Wang, Z., Fu, J. S., Wang, X., Itahashi, S., Yamaji, K., Nagashima,
808 T., Lee, H.-J., Kim, C.-H., Lin, C.-Y., Chen, L., Zhang, M., Tao, Z., Li, J., Kajino, M., Liao,
809 H., Sudo, K., Wang, Y., Pan, Y., Tang, G., Li, M., Wu, Q., Ge, B., and Carmichael, G. R.:
810 Evaluation and uncertainty investigation of the NO₂, C and NH₃ modeling over China under
811 the framework of MICS-Asia III, *Atmos. Chem. Phys. Discuss.*, [http://doi.org/10.5194/acp-
2018-1158](http://doi.org/10.5194/acp-

812 2018-1158), **accepted**, 2019.

813 Krotkov, N. A., McLinden, C. A., Li, C., Lamsal, L. N., Celarier, E. A., Marchenko, S. V., Swartz,
814 W. H., Bucsela, E. J., Joiner, J., Duncan, B. N., Boersma, K. F., Veefkind, J. P., Levelt, P.
815 F., Fioletov, V. E., Dickerson, R. R., He, H., Lu, Z., and Streets, D. G.: Aura OMI

Deleted: in review

817 observations of regional SO₂ and NO₂ pollution changes from 2005 to 2015, *Atmos. Chem.*
818 *Phys.*, 16(7), 4605–4629, doi:10.5194/acp-16-4605-2016, 2016.

819 Kumar, S. V., Peters-Lidard, C. D., Tian, Y., Houser, P. R., Geiger, J. Olden, S., Lighty, L.,
820 Eastman, J. L., Doty, B., Dirmeyer P., Adams, J., Mitchell K., Wood, E. F., and Sheffield, J.:
821 Land Information System – An Interoperable Framework for High Resolution Land Surface
822 Modeling, *Environ. Modelling & Software*, 21, 1,402-1,415, 2006.

823 Kuang, S., Newchurch, M. J., Burris, J., Wang, L., Buckley, P. I., Johnson, S., Knupp, K., Huang,
824 G., Phillips, D., and Canrell, W.: Nocturnal ozone enhancement in the lower troposphere
825 observed by lidar, *Atmos. Environ.*, 45, 6078-6084, 2011.

826 Lee, S. S. Li, Z., Zhang, Y. Yoo, H., Kim, S., Kim, B.-G., Choi, Y.-S., Mok, J., Um, J., Choi, K.
827 O., and Dong, D.: Effects of model resolution and parameterizations on the simulations of
828 clouds, precipitation, and their interactions with aerosols, *Atmos. Chem. Phys.*, 18, 13–29,
829 doi:10.5194/acp-18-13-2018, 2018.

830 Lelieveld, J., Evans, J. S., Fnais, M., Giannadaki D., and Pozzer, A.: The contribution of outdoor
831 air pollution sources to premature mortality on a global scale, *Nature*, 525, 367-371, 2015.

832 Li, J., Nagashima, T., Kong, L., Ge., B., Yamaji, K., Fu, J. S., Wang, X., Fan, Q., Itahashi, S., Lee,
833 H.-J., Kim, C.-H., Lin, C.-Y., Zhang, M., Tao, Z., Kajino, M., Liao, H., Li, M., Woo, J.-H.,
834 Kurokawa, J., Wang, Z., Wu, Q., Akimoto, H., Carmichael, G. R., and Wang, Z.: Model
835 evaluation and intercomparison of surface-level ozone and relevant species in East Asia in the
836 context of MICS-Asia phase III, Part I: overview, *Atmos. Chem. Phys.*, 19, 12993-13015,
837 <http://doi.org/10.5194/acp-19-12993-2019>, 2019.

838 Li, M., Zhang, Q., Kurokawa, J. I., Woo, J. H., He, K., Lu, Z., Ohara, T., Song, Y., Streets, D. G.,
839 Carmichael, G. R., Cheng, Y., Hong, C., Huo, H., Jiang, X., Kang, S., Liu, F., Su, H., and
840 Zheng, B.: MIX: a mosaic Asian anthropogenic emission inventory under the international
841 collaboration framework of the MICS-Asia and HTAP, *Atmos. Chem. Phys.*, 17, 935-963,
842 doi:10.5194/acp-17-935-2017, 2017.

843 Lin, M., Holloway, T., Carmichael, G. R., and Fiore, A. M.: Quantifying pollution inflow and
844 outflow over East Asia in spring with regional and global models, *Atmos. Chem. Phys.*, 10,
845 4221-4239, doi: 10.5194/acp-10-4221-2010, 2010.

846 Lu, X., Hong, J., Zhang, L., Cooper, O. R., Schultz, M. G., Xu, X., Wang, T., Gao, M., Zhao, Y.,
847 and Zhang, Y.: Severe surface ozone pollution in China: A global perspective, *Environ. Sci.*
848 *Technol. Lett.*, 5, 487-494, 2018.

849 Matsui, T., Tao, W.-K., Masunaga, H., Kummerow, C. D., Olson, W. S., Teruyuki, N., Sekiguchi,
850 M., Chou, M., Nakajima, T. Y., Li, X., Chern, J., Shi, J. J., Zeng, X., Posselt, D. J., and
851 Suzuki, K.: Goddard Satellite Data Simulation Unit: Multi-Sensor Satellite Simulators to
852 Support Aerosol- Cloud-Precipitation Satellite Missions, *Eos Trans.*, 90(52), Fall Meet.
853 *Suppl.*, Abstract A21D-0268, 2009.

854 Matsui, T., Iguchi, T., Li, X., Han, M., Tao, W.-K., Petersen, W., L'Ecuyer, T., Meneghini, R.,
855 Olson, W., Kummerow, C. D., Hou, A. Y., Schwaller, M. R., Stocker, E. F., and Kwiatkowski,
856 J.: GPM satellite simulator over ground validation sites, *Bull. Am. Meteor. Soc.*, 94, 1653-
857 1660, doi:10.1175/BAMS-D-12-00160.1, 2013.

858 Matui, T., Santanello, J., Shi, J. J., Tao, W.-K., Wu, D., Peters-Lidard, C., Kemp, E., Chin, M.,
859 Starr, D., Sekiguchi, M., and Aires, F.: Introducing multi-sensor satellite radiance-based
860 evaluation for regional earth system modeling, *J. Geophys. Res.*, 119, 8450-8475,
861 doi:10.1002/2013JD021424, 2014.

862 Maurer, E. P., Wood, A. W., Adam, J. C., Lettenmaier, D. P., and Nijssen, B.: A long-term

Deleted: -I.

Deleted: -

Deleted: . Discuss.

Field Code Changed

Deleted: 2018-1283, in review,

Formatted: Default Paragraph Font, Font: (Default) +Body (Calibri)

867 hydrologically based dataset of land surface fluxes and states for the continuous United State,
868 *J. Clim.*, 15(22), 3,237-3,251, 2002.

869 Mu, M., Randerson, J. T., van der Werf, G. R., Giglio, L., Kasibhatla, P., Morton, D., Collatz, G.
870 J., DeFries, R. S., Hyer, E. J., Prins, E. M., Griffith, D. W. T., Wunch, D., Toon, G. C.,
871 Sherlock, V., and Wennberg, P. O.: Daily and 3-hourly variability in global fire emissions
872 and consequences for atmospheric model prediction of carbon monoxide, *J. Geophys. Res.*,
873 116, D24303, doi:10.1029/2011JD016245, 2011.

874 Neal, L. S., Dalvi, M., Folberth, G., McInnes, R. N., Agnew, P., O'Connor, F. M., Savage, N. H.,
875 and Tilbee, M.: A description and evaluation of an air quality model nested within global
876 and regional composition-climate models using MetUM, *Geosci. Model Dev.*, 10, 3941-3962,
877 doi:10.5194/gmd-10-3941-2017, 2017.

878 Peters-Lidard, C. D., Houser, P. R., Tian, Y., Kumar, S. V., Geiger, J., Olden, S., Lighty, L., Doty,
879 B., Dirmeyer, P., Adams, J., Mitchell, K., Wood, E. F., and Sheffield, J.: High-performance
880 Earth system modeling with NASA/GSFC's Land Information System, *Innovations in
881 Systems and Software Engineering*, 3, 157–165, 2007.

882 Peters-Lidard, C. D., Kemp, E. M., Matsui, T., Santanello, J. A., Kumar, S. V., Jacob, J. P., Clune,
883 T., Tao, W.-K., Chin, M., Hou, A., Case, J. L., Kim, D., Kim, K.-M., Lau, W., Liu, Y., Shi,
884 J., Starr, D., Tan, Q., Tao, Z., Zaitchik, B. F., Zavodsky, B., Zhang, S. Q., and Zupanski,
885 M.: Integrated modeling of aerosol, cloud, precipitation and land processes at satellite-
886 resolved scales. *Environmental Modeling & Software* 67, 149-159, 2015.

887 Rienecker, M. M., Suarez, M. J., Gelaro, R., Todling, R., Bacmeister, J., Liu, E., Bosilovich, M.
888 G., Schubert, S. D., Takacs, L., Kim, G.-K., Bloom, S., Chen, J., Collins, D., Conaty, A., da
889 Silva, A., Gu, W., Joiner, J., Koster, R. D., Lucchesi, R., Molod, A., Owens, T., Pawson, S.,
890 Pegion, P., Redder, C. R., Reichle, R., Robertson, F. R., Ruddick, A. G., Sienkiewicz, M.,
891 and Woollen, J.: MERRA - NASA's Modern-Era Retrospective Analysis for Research and
892 Applications, *J. Climate*, 24, 3624–3648, 2011.

893 Seo, J., Youn, D., Kim, J. Y., and Lee, H.: Extensive spatiotemporal analyses of surface ozone and
894 related meteorological variables in South Korea for the period 1999-2010, *Atmos. Chem.
895 Phys.*, 14, 6395-6415, doi:10.5194/acp-14-6395-2014, 2014.

896 Shi, J. J., Matsui, T., Tao, W.-K., Tan, Q., Peters-Lidard, C. D., Chin, M., Pickering, K., Guy, N.,
897 Lang, S., and Kemp, E. M.: Implementation of an aerosol-cloud microphysics-radiation
898 coupling into the NASA Unified WRF: Simulation results for the 6-7 August 2006 AMMA
899 Special Observing Period, *Q. J. R. Meteorol. Soc.*, doi:10.1002/qj.2286, 2014.

900 Stockwell, W. R., Middleton, P., Chang, J. S., and Tang, X.: The Second Generation Regional
901 Acid Deposition Model Chemical Mechanism for Regional Air Quality Modeling, *J.
902 Geophys. Res.*, 95, 16343-16367, 1990.

903 Tao, W.-K., Shi, J. J., Chen, S. S., Lang, S., Lin, P.-L., Hong, S.-Y., Peters-Lidard, C., and Hou,
904 A.: The impact of microphysical schemes on hurricane intensity and track, *Asia-Pacific J.
905 Atmos. Sci.*, 47, 1–16, 2011.

906 Tao, Z., Santanello, J. A., Chin, M., Zhou, S., Tan, Q., Kemp, E. M., and Peters-Lidard, C. D.:
907 Effect of land cover on atmospheric processes and air quality over the continental United
908 States – A NASA Unified WRF (NU-WRF) model study, *Atmos. Chem. Phys.*, 13, 6207-
909 6226, doi: 10.5194/acp-13-6207-2013, 2013.

910 Tao, Z., Yu, H., and Chin, M.: Impact of transpacific aerosol on air quality over the United States:
911 A perspective from aerosol-cloud-radiation interactions, *Atmos. Environ.*, 125, 48-60,
912 doi:10.1016/j.atmosenv.2015.10.083, 2016.

913 Tao, Z., Braun, S. A., Shi, J. J., Chin, M., Kim, D., Matsui, T., and Peters-Lidard, C. D.:
914 Microphysics and radiation effect of dust on Saharan air layer: An HS3 case study, *Mon. Wea.*
915 *Rev.*, 146, 1813-1835, doi:10.1175/MWR-D-17-0279.1, 2018.

916 Tie, X., Brasseur, G., and Ying, Z.: Impact of model resolution on chemical ozone formation in
917 Mexico City: application of the WRF-Chem model, *Atmos. Chem. Phys.*, 10, 8983-8995,
918 doi:10.5194/acp-10-8983-2010, 2010.

919 Valari, M. and Menut, L.: Does an increase in air quality model's resolution bring surface ozone
920 concentrations closer to reality?, *J. Atmos. Oceanic Tech.*, 25, 1955-1968,
921 doi:10.1175/2008JTECHA1123.1, 2008.

922 van der Werf, G. R., Randerson, J. T., Giglio, L., Collatz, G. J., Mu, M., Kasibhatla, P. S.,
923 Morton, D. C., DeFries, R. S., Jin, Y., and van Leeuwen, T. T.: Global fire emissions and the
924 contribution of deforestation, savanna, forest, agricultural, and peat fires (1997–2009),
925 *Atmos. Chem. Phys.*, 10, 11707-11735, doi:10.5194/acp-10-11707-2010, 2010.

926 Wang, W.-N., Cheng, T.-H., Gu, X.-F., Chen, H., Guo, H., Wang, Y., Bao, F.-W., Shi, S.-Y., Xu,
927 B.-R., Zuo, X., Meng, C., and Zhang, X.-C.: Assessing spatial and temporal patterns of
928 observed ground-level ozone in China, *Sci. Rep.*, 7, 3651, doi:10.1038/s41598-017-03929-
929 w, 2017.

930 Yu, Man: An assessment of urbanization impact on China by using WRF-Chem and configuration
931 optimization, PhD (Doctor of Philosophy) thesis, University of Iowa,
932 <https://doi.org/10.17077/etd.lzfu2tj8>, 2014.

933 Zhao, X. J., Zhao, P. S., Xu, J., Meng, W., Pu, W. W., Dong, F., He, D., and Shi, Q. F.: Analysis
934 of a winter regional haze event and its formation mechanism in the North China Plain, *Atmos.*
935 *Chem. Phys.*, 13, 5685-5696, doi:10.5194/acp-13-5685-2013, 2013.

936 Zou, Y., Wang, Y., Zhang, Y., and Koo, J.-H.: Arctic sea ice, Eurasia snow, and extreme winter
937 haze in China, *Sci. Adv.*, 3, e1602751, 2017.

938
939
940
941
942

943 Table 1. Information of Air Quality Observation Sites
 944

Site Name	Symbol	Longitude	Latitude	Altitude (m)	Setting
Baoding	BD	115.441	38.824	4	Urban
Beijing Tower	BJT	116.372	39.974	44	Urban
Chengde	CD	117.925	40.973	395	Urban
Caofeidian	CFD	118.442	39.270	11	Urban
Cangzhou	CZ	116.779	38.286	12	Urban
Datong	DT	113.389	40.089	1058	Urban
Gu An	GA	115.734	39.149	21	Rural
Hejian	HJ	116.079	38.423	66	Urban
Hengshui	HS	115.656	37.742	77	Urban
Langfang	LF	116.689	39.549	19	Urban
Lingshan	LS	115.431	39.968	116	Rural
Longtan Lake	LTH	116.430	39.870	31	Urban
Qian An	QA	118.800	40.100	54	Urban
Qinhuangdao	QHD	119.570	39.950	2.4	Urban
Shijiazhuang	SJZ	114.529	38.028	70	Urban
Shuangqing Road	SQL	116.338	40.007	58	Urban
Tanggu	TG	117.717	39.044	13	Urban
Tianjin	TJ	117.206	39.075	2	Urban
Tangshan	TS	118.156	39.624	14	Urban
Xianghe	XH	116.962	39.754	9	Suburban
Xinglong	XL	117.576	40.394	879	Rural
Yangfang	YF	116.126	40.147	78	Suburban
Yanjiao	YJ	116.824	39.961	26	Suburban
Zhangjiakou	ZJK	114.918	40.771	777	Urban
Zhuozhou	ZZ	115.988	39.460	48	Suburban

945
 946
 947
 948
 949
 950

Table 2. Comparisons of occurrences of exceedances of China's National Ambient Air Quality Standards between observations and simulations*

	Frequency	Class 1	Class 2	Obs.	45-km	15-km	5-km
CO	Hourly	10	10	1,150	0	0	0
O ₃	Hourly	160	200	3,684	24,807	10,283	9,880
NO _x	Hourly	250	250	9,009	14	520	3,003
SO ₂	Hourly	150	500	393	0	2	39
PM _{2.5}	24-hours	35	75	1,343	1,720	1,610	1,574
PM ₁₀	24-hours	50	150	2,834	2,067	1,617	1,676

951
 952
 953
 954

* Class 1/2 standards are for rural/suburban-urban, respectively. Units are **ppbm** for CO, **ppbv** for O₃, NO_x, and SO₂, and **µg m⁻³** for PM_{2.5} and PM₁₀.

Formatted: Subscript
 Formatted: Subscript
 Deleted: .

956
 957
 958

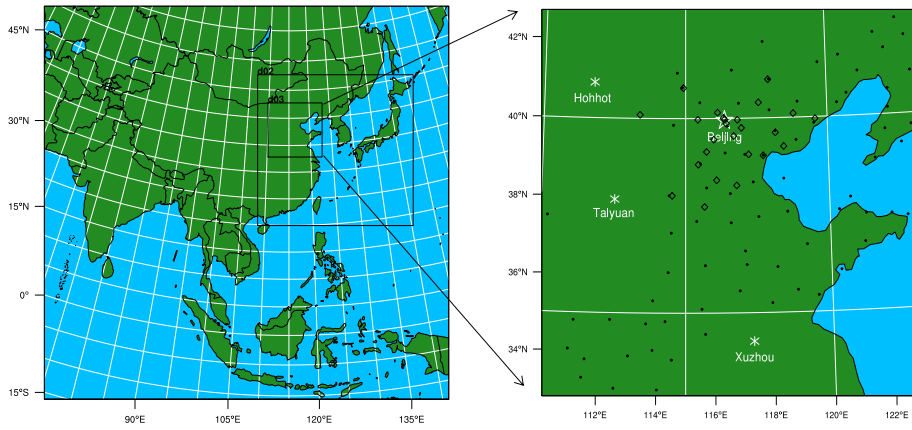
Table 3. Domain total emissions and average meteorology and air quality at various resolutions

Deleted: Regional

Variables	Period	45-km	15-km	5-km
Biogenic Isoprene (tons)	Annual	740,562	869,317	862,199
Dust (tons)	Annual	2,431	4,485	3,910
Sea salt (tons)	Annual	548	1,287	1,417
Surface air temperature (K)	January	268	267	268
	July	300	299	299
Surface wind speed (m s ⁻¹)	January	2.92	2.73	2.51
	July	1.70	1.54	1.52
SWDOWN (W m ⁻²)	January	124	117	117
	July	249	242	250
PBLH (m)	January	333	338	331
	July	627	595	574
CWP (g m ⁻²)	January	4.34	11.3	11.1
	July	41.4	56.8	55.2
Surface O ₃ (ppbv)	January	37.5	39.4	39.5
	July	86.8	68.8	69.2
Surface NO _x (ppbv)	January	19.8	14.9	15.0
	July	9.03	8.32	7.96
Surface CO (ppmv)	January	0.600	0.521	0.526
	July	0.444	0.336	0.308
Surface SO ₂ (ppbv)	January	16.6	12.9	13.2
	July	10.2	6.55	6.23
Surface PM _{2.5} (µg m ⁻³)	January	70.9	59.8	61.0
	July	89.3	58.0	46.2
Surface PM ₁₀ (µg m ⁻³)	January	102	88.1	89.6
	July	108	74.9	60.3

959
 960

962



963

964

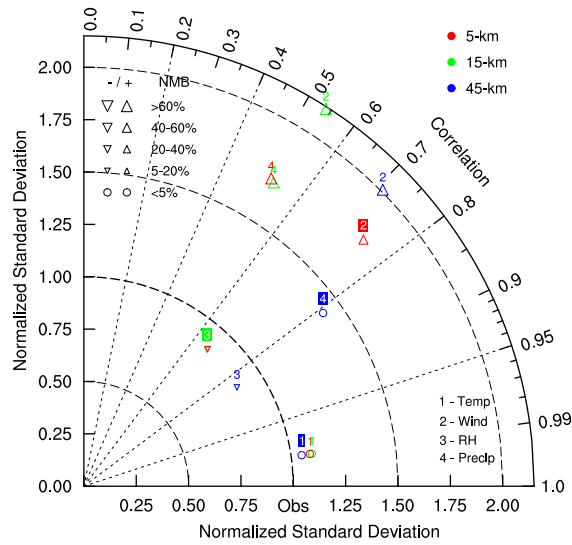
965 Figure 1. NU-WRF domain set-up. Left panel is the nested MICS-Asia domains; right panel is the
966 enlarged NCP domain (d03) with diamonds representing the air quality monitoring sites and black
967 dots denoting for the meteorological stations. Locations of four cities are marked for position
968 reference.

969

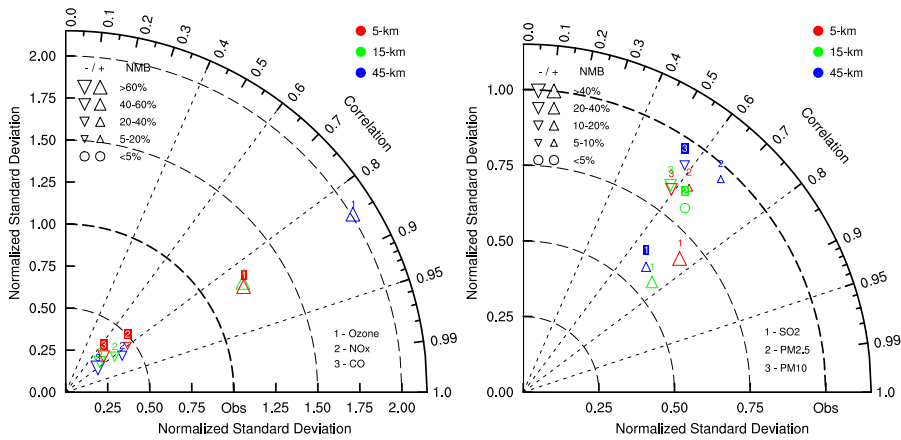
970

971

972



973



974

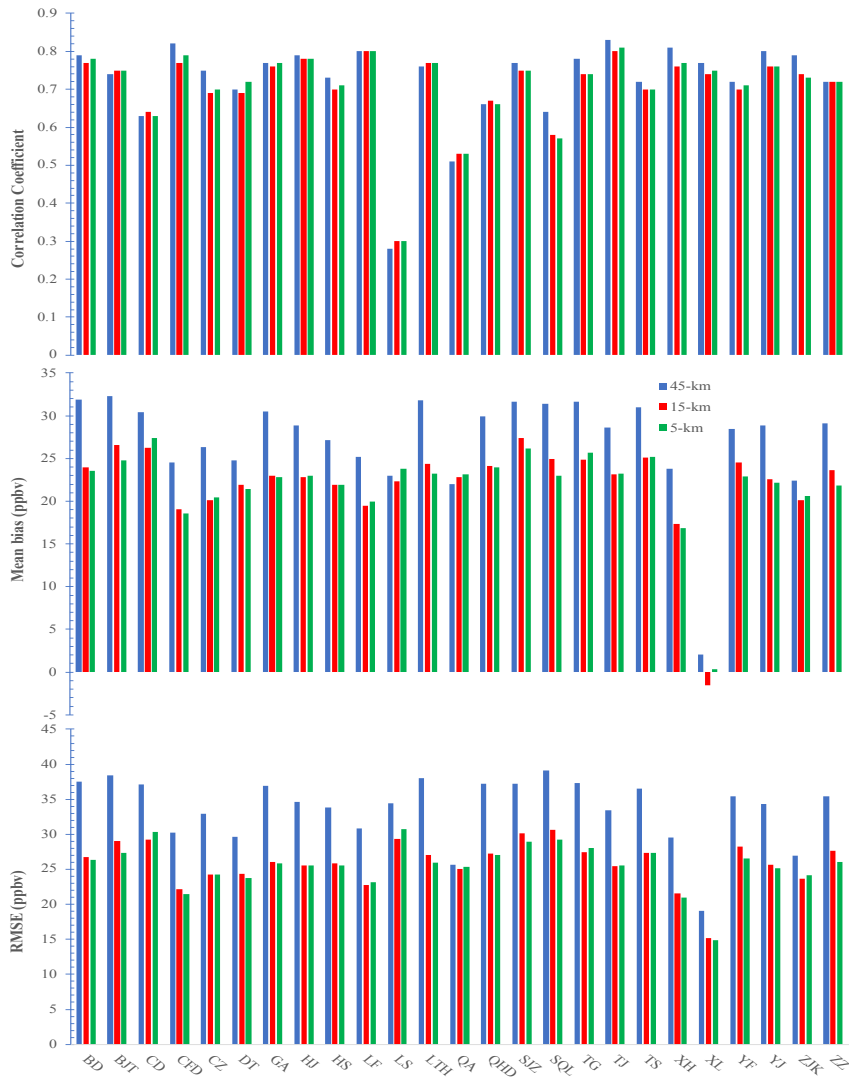
975

976 Figure 2. Taylor diagram for evaluations of NU-WRF performances on meteorology (top row) and
977 air quality (bottom row) simulations at three resolutions

978

979

980



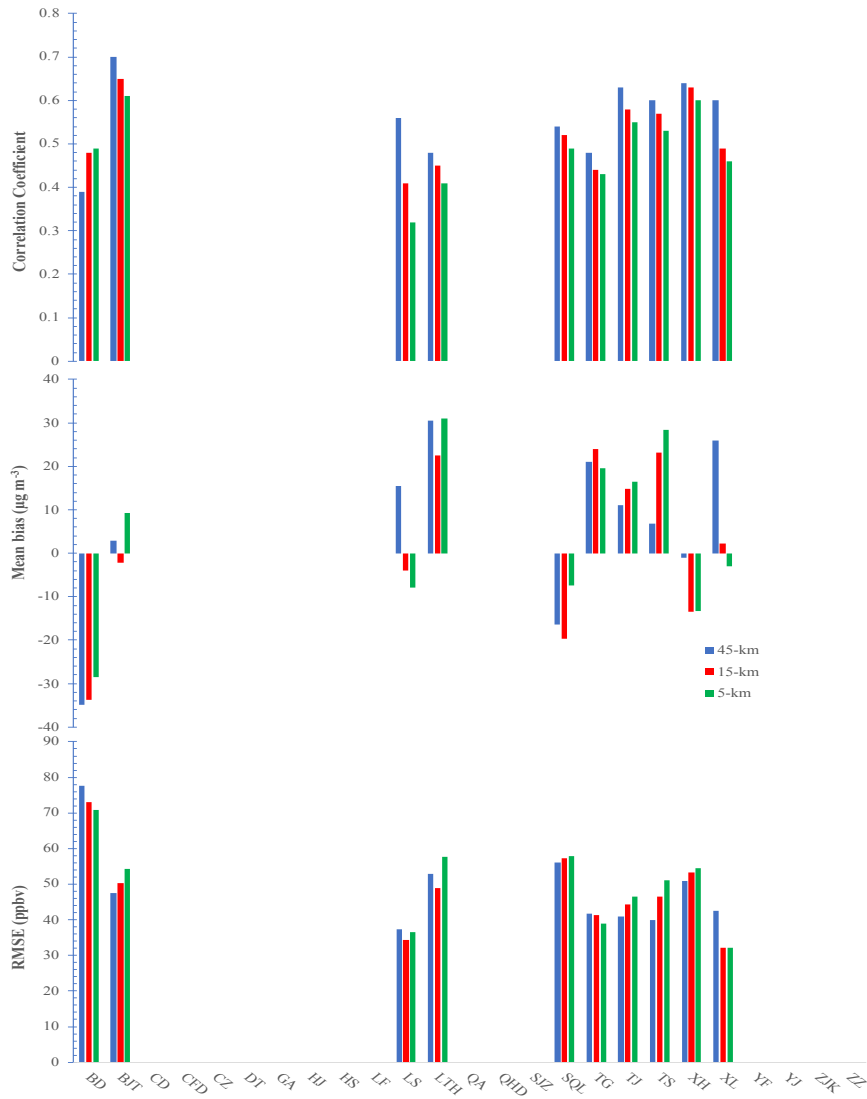
981

982

983 Figure 3. Comparisons of *MB*, *RMSE*, and correlation coefficient (*r*) of surface O₃ from different
984 horizontal resolutions at each air quality monitoring site

985

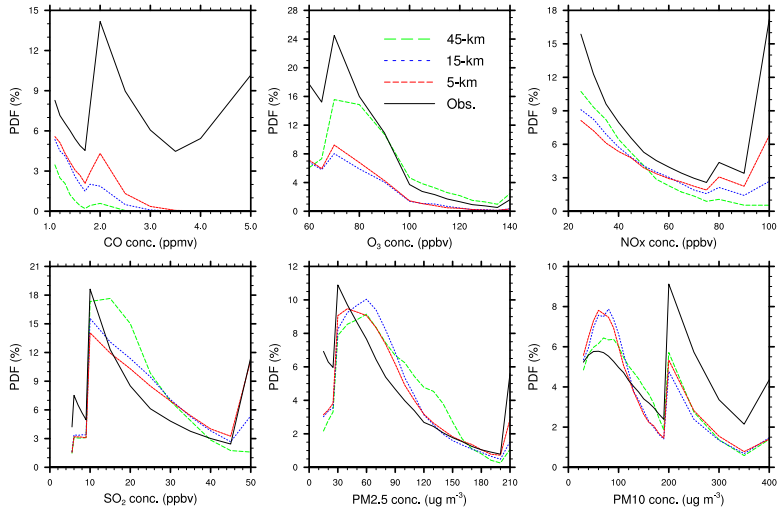
986



987
988
989
990
991

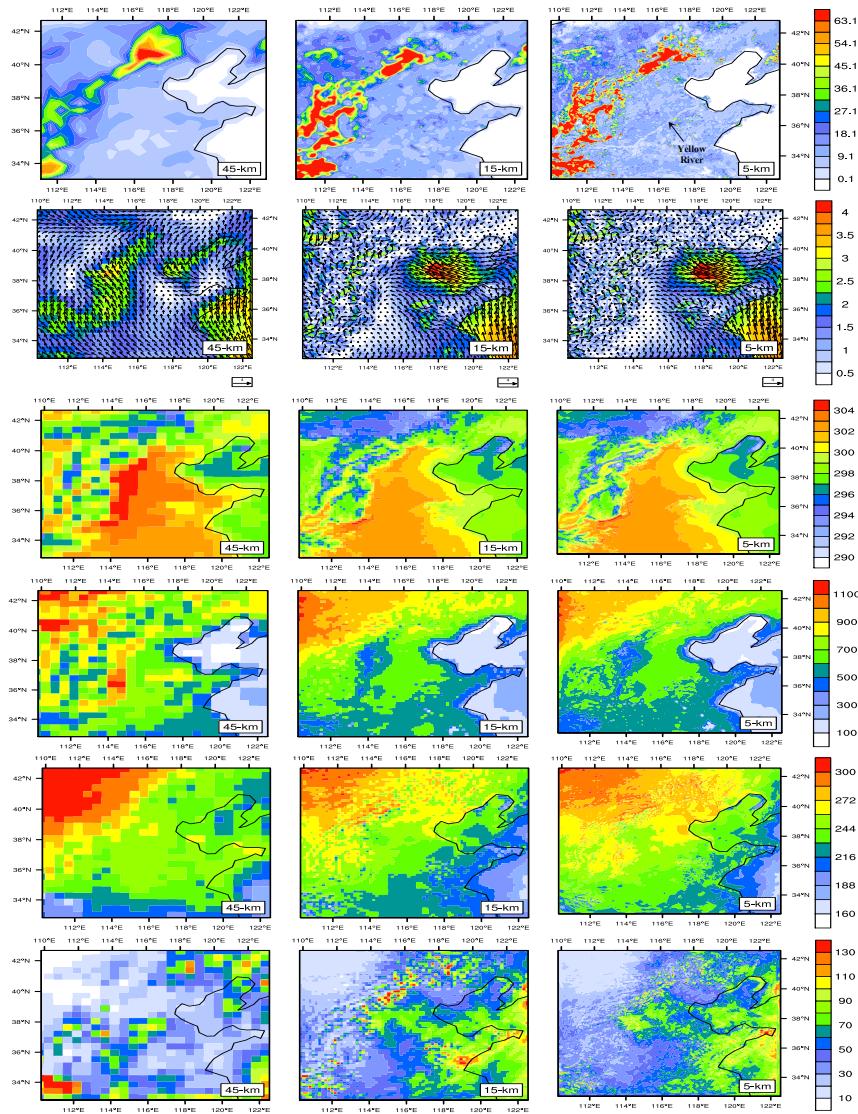
Figure 4. Comparisons of *MB*, *RMSE*, and correlation coefficient (*r*) of surface PM_{2.5} from different horizontal resolutions at each air quality monitoring site (blank space indicates no data are available)

992

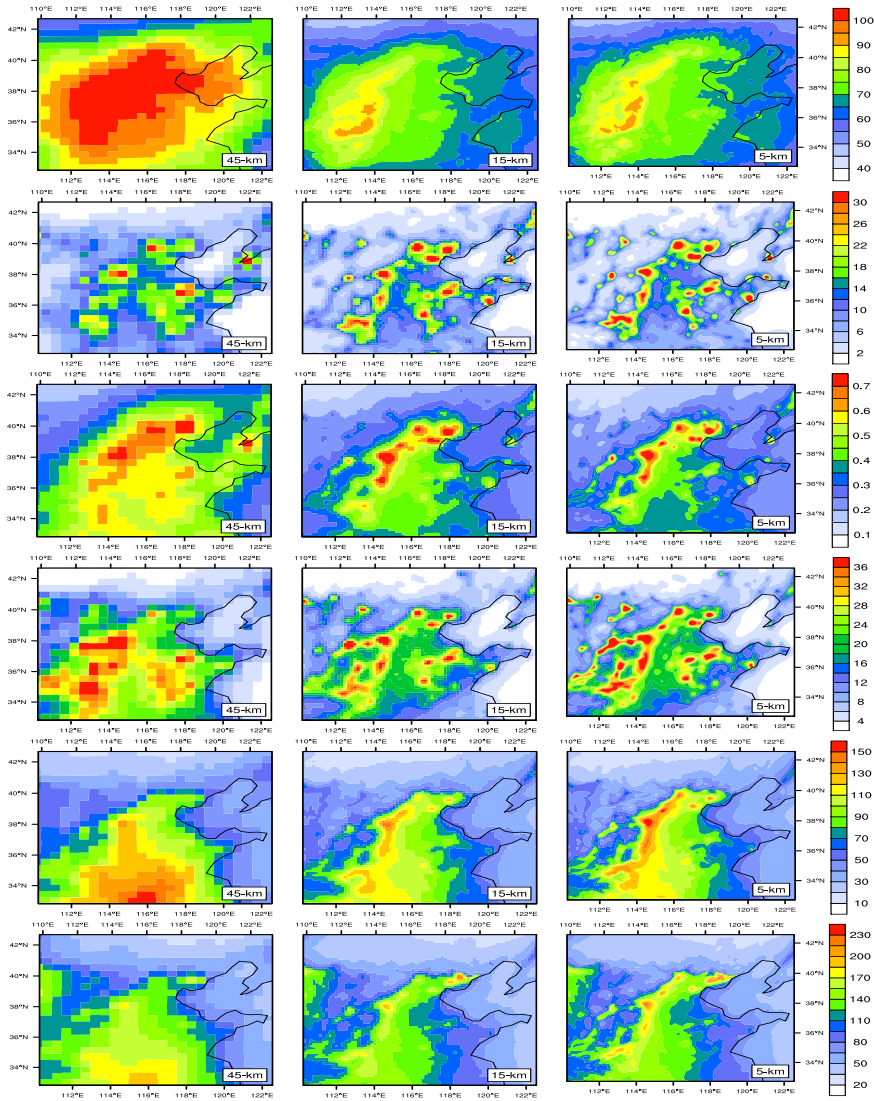


993
994
995
996

Figure 5. Probability density function (PDF) plots for hourly concentrations of surface air quality

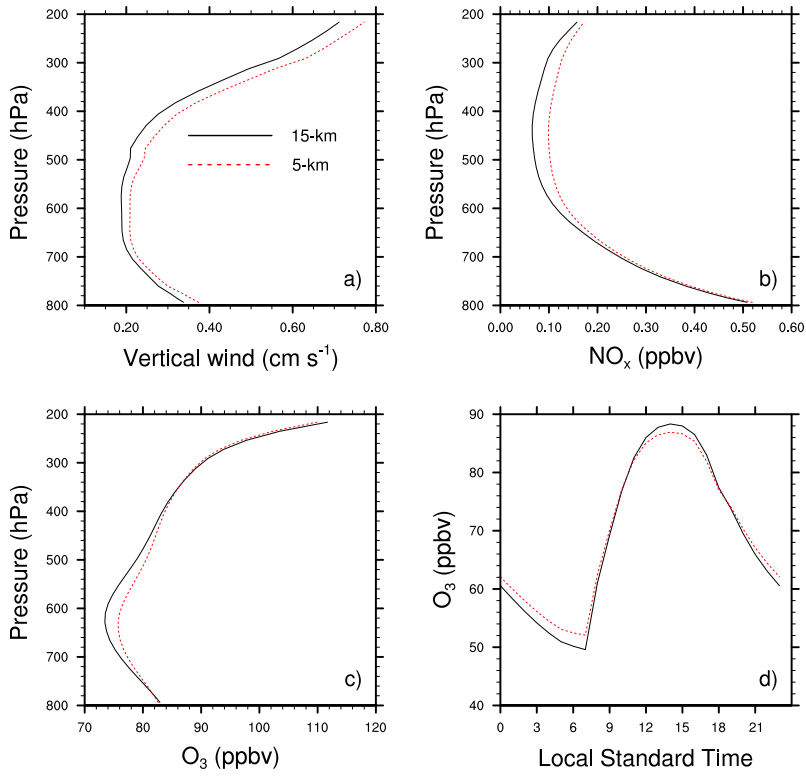


997
 998 Figure 6. Simulated emissions and July average meteorology from 3 grids: 1st row = isoprene
 999 emissions ($\text{mol km}^{-2} \text{hr}^{-1}$) from biogenic sources on a typical summer day; 2nd row = surface wind
 1000 vector with the shade representing wind speed (m s^{-1}); 3rd row = surface air temperature (K); 4th
 1001 row = PBLH (m); 5th row = SWDOWN (W m^{-2}); 6th row = CWP (g m^{-2}).
 1002



1003
1004
1005
1006
1007
1008

Figure 7. Simulated January (SO_2 , $\text{PM}_{2.5}$, and PM_{10}) and July (O_3 , NO_x , and CO) surface average air quality from 3 grids: 1st row = O_3 (ppbv); 2nd row = NO_x (ppbv) 3rd row = CO (ppmv); 4th row = SO_2 (ppbv); 5th row = $\text{PM}_{2.5}$ ($\mu\text{g m}^{-3}$); 6th row = PM_{10} ($\mu\text{g m}^{-3}$).



1009
1010
1011
1012

Figure 8. Domain average profiles of vertical wind, NO_x, and O₃ concentrations (Panels a-c) and domain average diurnal variations of surface O₃ over July.